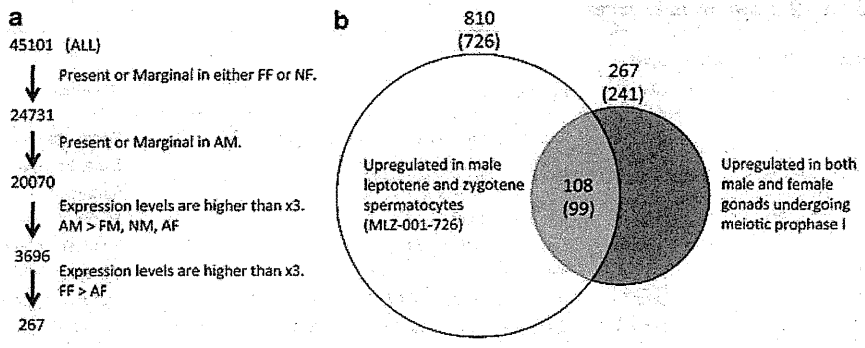

Figure 1 Generation of a gene set that is upregulated during meiotic prophase I. (**a**) Strategy for filtering genes that are upregulated in the mouse gonads undergoing meiotic prophase I. 'Present' and 'Marginal' are detection calls of the MAS5 algorithm, which is an indicator of expression. The numbers of genes selected by each step are indicated. (**b**) Venn diagram indicating the number of selected genes using two criteria: the MLZ gene set identified previously by Kogo *et al.*[14] (left) and genes identified in the current analysis (right).

Table 1 Classification of 99 (241)[a] candidate meiotic genes from the mouse

Genes	*Characteristics*	*Number*	*Subtotal*	*Total*
Known	Meiosis-preferred expression	17 (20)		
	Testis-preferred expression	6 (6)		
	Others	53 (157)	76 (183)	
Unknown	Others	23 (58)	23 (58)	99 (241)

[a]Numbers in the parentheses are that of the 241 gene set.

well-known functional association with chromosomal behavior in meiosis, did not appear among these 99 genes, but were included in the initial screen of 241 genes. We thus performed subsequent analyses also on this larger 241 gene set.

Developmental gene expression profiling of the female mouse gonads

To explore which of the candidate genes in our data sets show a similar expression profile with known meiotic genes, we grouped the 241 and 99 gene panels discretely into 4 clusters using k-means clustering analysis. Three groups of microarray data from mouse female gonads were applied to this analysis in order to focus on the expression level changes between the early (15.5 dpc) and late (neonatal day 1) stages of prophase I. The results of our clustering of the 241 genes are shown in Figure 2a and Supplementary Table 2. For the genes in cluster A, the expression levels are higher in NF than in FF or AF. Fifty genes were grouped in cluster A, but none with known functions in meiotic chromosomal behavior and only 11 that overlapped with the 99 selected meiotic genes. Hence, cluster A appeared to contain female-predominant genes expressed in the later stages of oogenesis. Cluster B contained as many as 110 genes, but only five with meiosis-specific expression, suggesting that many of the genes in this cluster may not be specifically associated with meiotic chromosomal behavior. The gene expression patterns for cluster C were found to be similar to those of cluster B, although the expression levels in FF were higher than the genes in cluster B. Cluster C contains 10 meiotic genes including *Spo11*, *Rec8* and *Sycp3*. Genes in cluster D exhibited the highest expression levels in FF compared with the other clusters. Among the 27 genes in this cluster, 22 overlapped with the 99 gene panel, and five of these genes are well-known meiotic genes including *Dmc1* and *Smc1b*. These results confirm the enrichment of genes involved in meiosis I prophase in the 99 gene set.

Similar clustering was also performed for the 99 selected genes (Figure 2b and Supplementary Table 3). The expression levels of the genes assigned to cluster 1 were high in FF but decreased in NF. *Spo11*, *Dmc1* and *Atm*, which are the key enzymes involved in the formation and repair of meiotic DNA double-strand breaks, were included in this cluster. The expression levels of the genes in cluster 2 were higher in both FF and NF than those of the cluster 1 genes. This cluster includes a cohesin component, *Smc1b*. Hence, clusters 1 and 2 may include genes involved in early stages of prophase during meiosis I. Cluster 3 contains genes whose expression did not switch off until neonatal day 1. *Sycp1*, *Sycp3* and *Syce1* are included in this cluster, which indicates that the genes in cluster 3 are necessary through to the later stages of prophase I. The genes in cluster 4 showed lower expression in both FF and NF than the genes of any other clusters. *Syce2* is the only gene in this cluster to have been functionally established as a meiotic gene, indicating that our 99 gene panel still included non-meiotic genes that were categorized into cluster 4.

Real-time RT-PCR analysis of selected genes

We randomly selected nine genes from the 99 gene panel with no known function in meiosis (Table 3). These genes were analyzed by real-time RT-PCR to verify whether they were meiosis-specific (Figure 3). We used RNA extracts from the gonads of FM, FF, AM and AF mice, because we were focusing only on the early stages of prophase I. The expression of *Sycp3*, a meiosis-specific gene, showed high levels in FF and AM, but low levels in FM, AF and somatic tissues (Figure 3a). MLZ-175, MLZ-611, MLZ-638 and MLZ-675 showed meiotic expression patterns that were similar to *Sycp3* (Figure 3a). MLZ-254, MLZ-326 and MLZ-344 showed testis-predominant expression patterns (Figure 3b). MLZ-352 and MLZ-617 showed testis-predominant expression patterns, but were found to be expressed also in the adult mouse ovary (Figure 3b). In 11 of the known meiotic genes listed in Supplementary Table 3, the expression ratios of FF to AF derived from the microarray analysis were high (>22-fold). These genes ranked in the top 25 among the 99 gene panel in terms of the ratios of FF to AF. Among the nine genes we analyzed by real-time RT-PCR, MLZ-611 and MLZ-675 ranked also in the top 25, and both showed meiotic expression patterns (Figure 3a). These results suggest that genes with a higher expression ratio of FF to AF among our 99 selected genes are strong candidates as functional genes in meiotic chromosomal behavior.

Table 2 Microarray data for 12 known meiotic genes

Probe set ID	Fold change (FF/AF)	Rank in 99	Cluster in 99	Gene symbol	Description	Function	Expression
1449253_at	329.15	1	2	*Smc1b*	Structural maintenance of chromosomes 1B	Sister chromatid cohesion	Meiotic
1450292_a_at	130.82	6	1	*Hormad1*	HORMA domain containing 1	Synaptonemal complex formation	Meiotic
1460229_at	68.84	10	1	*Stag3*	Stromal antigen 3	Sister chromatid cohesion	Meiotic
1427291_at	52.27	12	3	*Sycp1*	Synaptonemal complex protein 1	Synapsis (central element)	Meiotic
1449534_at	35.78	14	3	*Sycp3*	Synaptonemal complex protein 3	Synapsis (lateral element)	Meiotic
1420335_at	27.29	19	1	*Dmc1*	Disrupted meiotic cDNA 1 homolog	Meiotic recombination	Meiotic
1453872_at	27.03	20	1	*Dmrtc2*	Doublesex- and mab-3-related transcription factor-like family C2	Sex chromatin transformation in male	Meiotic
1419511_at	23.93	24	1	*Msh4*	mutS homolog 4	Meiotic recombination	Meiotic
1417021_a_at	11.17	37	1	*Spo11*	Sporulation protein 11	Meiotic recombination	Meiotic
1429270_a_at	5.14	67	4	*Syce2*	Synaptonemal complex central element protein 2	Synapsis (central element)	Meiotic
1427197_at	4.12	74	1	*Atr*	Ataxia telangiectasia and Rad3 related	Meiotic recombination	Ubiquitous
1449170_at	3.03	99	3	*Piwil2*	piwi-like homolog 2	Gene regulation	Meiotic

Abbreviations: AF, 10-week-old female; FF, 15.5-dpc fetal female.

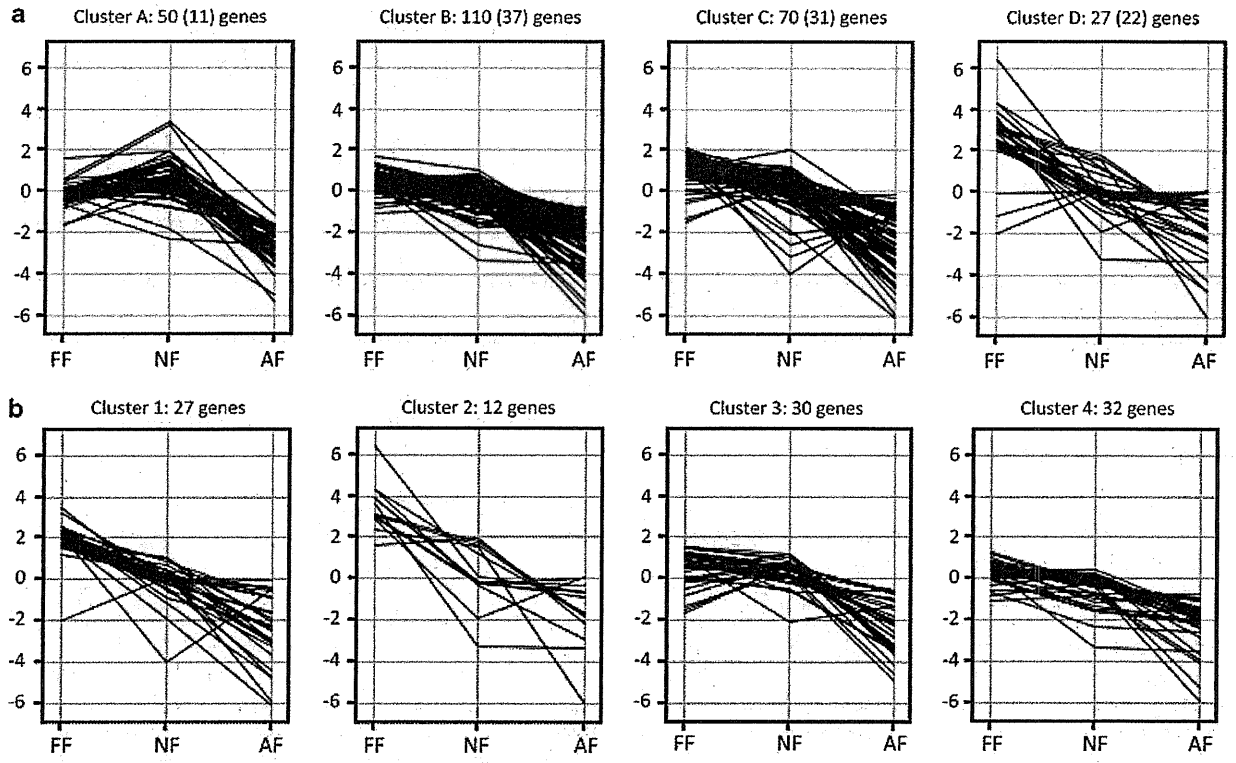

Figure 2 K-means clustering for the gene expression profiles of the 241 and 99 gene panels derived from the developmental mouse ovary. (**a**) Clustering of the 241 gene panel. Numbers indicate the gene numbers of the 241 panel, whereas those in parentheses denote the candidates in the 99 gene panel. (**b**) Clustering of the 99 gene panel. Numbers indicate the gene numbers of this panel. Normalized signal intensities are shown on the y axis. Because some genes have more than one probe set on the microarray platform, the sum of the four clusters exceeds 241 or 99 (see Supplementary Tables 2 and 3).

Subcellular localization of the epitope-tagged proteins expressed in mouse oocytes

To perform a further screen for meiotic genes that might be involved in chromosome segregation, we examined the subcellular localization of the protein products encoded by our candidate genes using vectors expressing epitope-tagged proteins. In our previous study, HEK293 cells had been used as a heterologous transfection system.[14] However, ectopically expressed SYCP3 generates a loop-like structure not only in the nucleus but also in the cytoplasm in somatic cell lines, which had not correctly reflected its intrinsic localization pattern in a previous report.[9] Therefore, in our current analyses we introduced a plasmid DNA expressing FLAG-tagged SYCP3 into adult mouse testis by *in vivo* electroporation. The FLAG-tagged SYCP3 protein product was detectable in the nuclei of pachytene spermatocytes by

Table 3 Validation results for nine of the candidate genes in this study

Name	Probe set ID	Fold change (FF/AF)	Rank in 99	Representative public ID	Gene symbol	Gene title	RT-PCR	Subcellular localization
MLZ-175	1423576_a_at	8.31	48	AV283456	*Fhl4*	Four and a half LIM domains 4	Meiotic	ND
MLZ-254	1429366_at	8.4	47	AK005720	*Lrrc34*	Leucine rich repeat containing 34	Testis	ND
MLZ-326	1426806_at	3.8	79	AV313559	*Obfc2a*	Oligonucleotide/oligosaccharide-binding fold containing 2A	Testis	ND
MLZ-344	1432386_a_at	6.85	55	AK005673	*Phf7*	PHD finger protein 7	Testis	ND
MLZ-352	1429936_at	5.94	62	BC019481	*Pih1d2*	PIH1 domain containing 2	Testis	ND
MLZ-611	1432458_at	196.87	3	AK005864	*1700011F14Rik*	RIKEN cDNA 1700011F14 gene	Meiotic	Nuclear and cytoplasm
MLZ-617	1436593_at	9.75	44	AV260052	*1700016K19Rik*	RIKEN cDNA 1700016K19 gene	Testis	ND
MLZ-638	1453942_at	11.58	35	AK007250	*1700123I01Rik*	RIKEN cDNA 1700123I01 gene	Meiotic	Cytoplasm
MLZ-675	1431648_at	58.82	11	AK015924	*4930528F23Rik*	RIKEN cDNA 4930528F23 gene	Meiotic	ND

Abbreviations: AF, 10-week-old female; FF, 15.5-dpc fetal female; ND, not determined.

immunofluorescence with anti-FLAG antibodies, and the staining pattern was found to be similar to that of endogenous SYCP3, reflecting that it is a component of the synaptonemal complex (Figure 4a). As we were focusing on the genes associated with female meiosis in the analysis, the same plasmid was introduced into a fetal mouse ovary by electroporation followed by *in vitro* organ culture. Overexpressed SYCP3 with a FLAG-tag was found to localize in the nuclei of leptotene oocytes as also demonstrated in spermatocytes (Figure 4b). These results indicate that epitope-tagged proteins that are overexpressed in both spermatocytes and oocytes show a pattern that reflects their intrinsic subcellular localization during meiosis. We thus applied this method to oocytes to examine the subcellular localization of unknown genes.

Plasmids expressing FLAG-tagged protein products for two candidate genes (MLZ-611 and MLZ-638) were introduced into oocytes (Figure 4b). The amino acid sequences encoded by these genes had no obvious nuclear localization signals and no distinct motifs other than coiled-coils. The protein encoded by MLZ-638 was observed in the cytoplasm of the oocytes. The localization of the MLZ-611 protein showed two patterns: both nuclear and cytoplasmic staining, and cytoplasmic only. The nuclear localization of MLZ-611 suggests a possible role in chromosome segregation.

DISCUSSION

To date, studies of global gene expression profiles of isolated oocytes have been mostly limited to metaphase II oocytes or earlier oocytes at the primordial follicle stage.[20–23] Although gene expression profile data for fetal or neonatal ovaries have been provided in mouse and human, and have enabled the analysis of genes involved in the initiation of meiosis, the sex differentiation of the gonad, early meiosis, and ovarian and follicle development, investigations of meiotic prophase I have been lacking.[24–28] In yeast, it is estimated that ~150 genes may be meiosis-specific.[29,30] In our current study, we screened 99 genes that are upregulated during prophase in meiosis I. Despite the fact that this gene number is less than one-seventh of the previous MLZ gene set, most of the well-known genes associated with meiotic chromosome behavior, sister chromatid cohesion, synapsis and homologous recombination, are included in this select gene panel. This indicates that our select 99 gene panel includes many other unknown meiotic genes, the functional elucidation of which will likely facilitate an increased understanding of the mechanisms underlying the sexual dimorphism between males and females. For further screening, 76 uncharacterized genes among these 99 genes is a reasonable number for individual validation by qRT-PCR. In addition, genes showing high FF to AF expression ratios by microarray should have priority in this respect.

Expression profiling using k-means clustering revealed that well-established meiotic genes were grouped into the same clusters, depending on their functions. Our clustering analysis of the initial 241 candidate gene panel showed that most of the known meiotic genes in this set grouped into two clusters, C and D. Hence, genes in these clusters that did not overlap with the 99 gene series may include genes that are upregulated after the zygotene stage and therefore warrant further analysis. Cluster 2, exhibiting the highest expression level in FF and NF among the four clusters established for the smaller 99 gene panel, included only one functionally known meiotic gene, *Smc1b*. This gene is important for maintaining the chiasma until adulthood, although its expression is clearly detectable only during the fetal stages and is barely evident in later stages in the female.[31] As the loading of SMC1B onto chromosomes begins at the leptotene stage during prophase I to establish meiotic cohesion, this protein needs to remain functional during a long meiotic arrest period in which it is not replenished.[19,32] The high expression of *Smc1b* transcripts in NF mice implies that robust cohesion might be established by this stage. A lack of turnover of the meiotic cohesin protein is considered to contribute to age-related chromosome segregation errors in oocytes.[32–34] The molecular mechanisms that maintain or disrupt meiotic cohesion have remained unclear for many decades. However, the candidate genes in cluster 2 in our current study may assist with our understanding of this complex phenomenon going forward.

Transient expression assays of epitope-tagged proteins to examine their subcellular localizations in oocytes would also likely assist with a determination of whether the molecules are engaged in chromosome behavior by direct observation of nuclear localization. The possible effect of the expression levels to the resultant subcellular localization might be overcome by observation of cells with various expression levels. As the efficiency of gene transfer for each gene varied from 2–3 cells to 20–30 cells per a litter, optimization of the condition for introduction might be necessary for each gene. To our knowledge, this is the first report to screen for genes of interest and then functionally characterize some of these candidates via their introduction into mouse oocytes during prophase I. Using this gene transfer system, the functions of uncharacterized gene can begin to be predicted if the localization of their encoded proteins is a unique nuclear domain, for

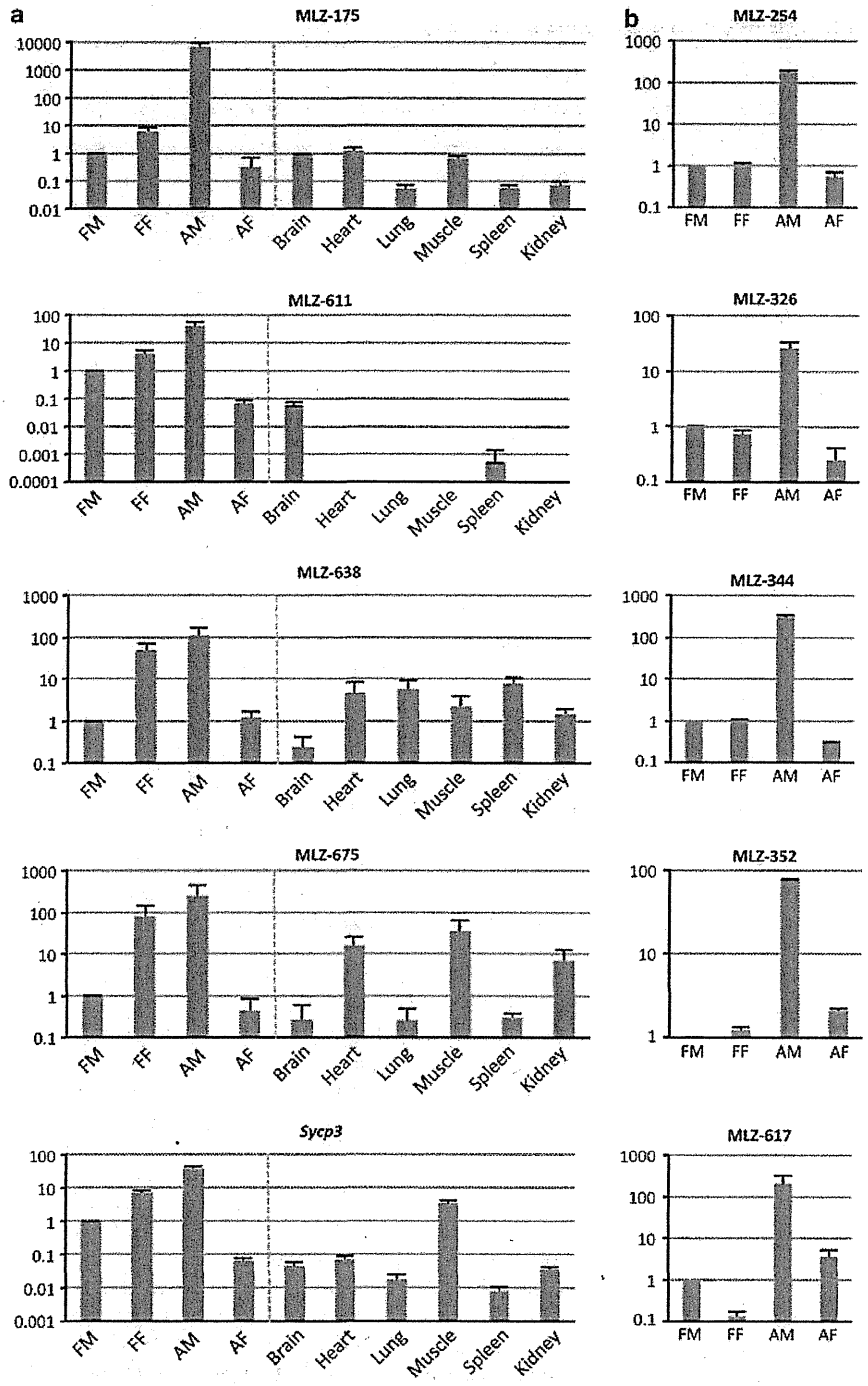

Figure 3 Real-time RT-PCR analysis of selected candidate genes using RNA from fetal gonads obtained from male and female mice at 15.5 dpc; adult gonads obtained from male and female mice at 10 weeks postpartum and somatic tissues. (**a**) Genes exhibiting meiotic expression patterns. (**b**) Genes exhibiting testis-predominant expression patterns. Expression ratios relative to the FM are shown on the y axis. Samples were run in triplicate, and error bars represent the standard deviation.

example, at the centromeres or chiasmata on meiotic chromosomes. Further, when a mutation has been identified in individuals with infertility or RPL, introduction of the mutant gene into oocytes in this way would readily enable functional analysis without the need to establish a knock-in mouse.

Also in our current analysis, we have identified that an uncharacterized gene, MLZ-611, may function in homologous chromosome segregation on the basis of its localization at the nucleus during prophase I. Recently, a bioinformatics approach using data from the published microarray analyses of gene expression during prophase I

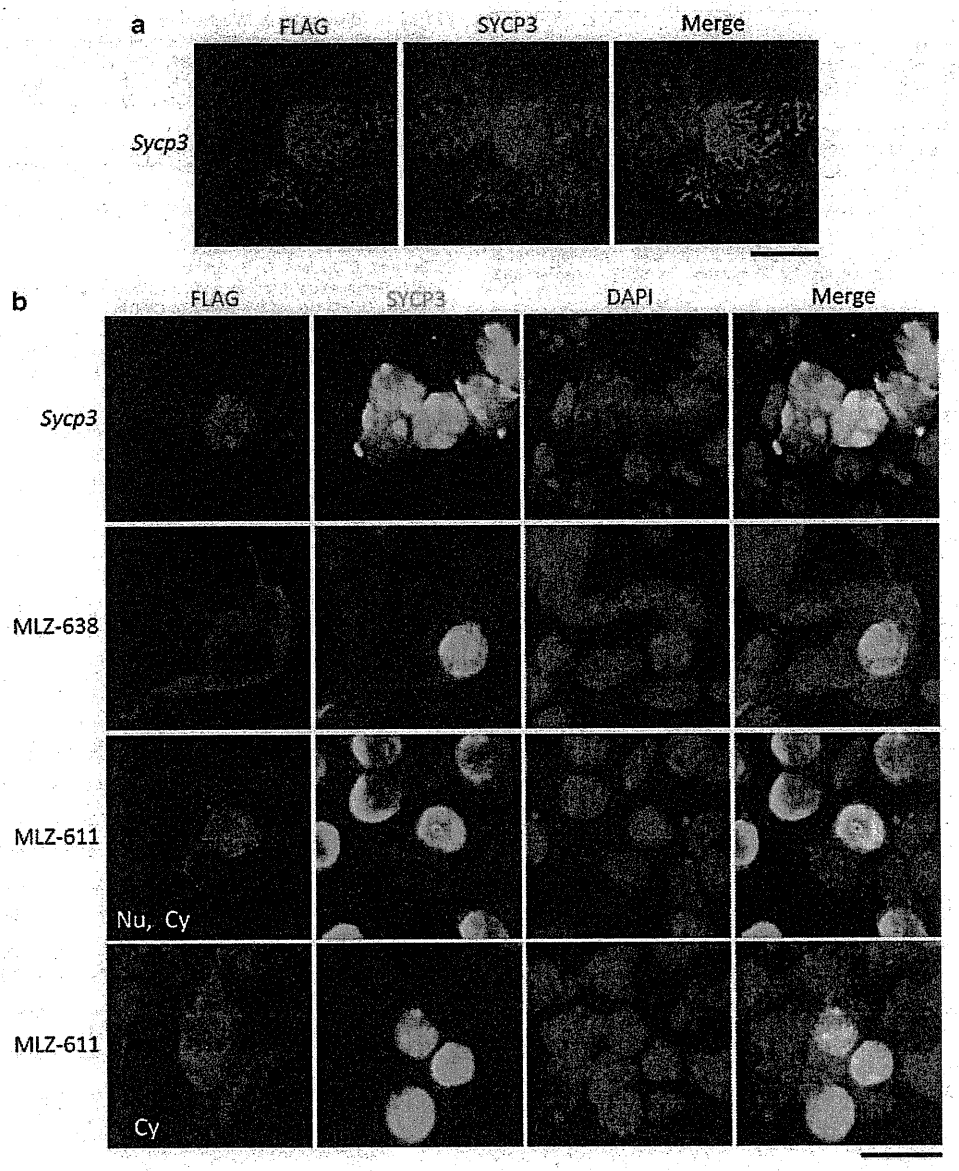

Figure 4 Subcellular localization of candidate meiotic gene protein products. Plasmids expressing FLAG-tagged proteins were introduced into mouse testis or ovarian tissues. (**a**) Immunostaining of testis frozen sections using anti-FLAG antibodies (red) and anti-SYCP3 antiserum (blue). Bar, 10 μm. (**b**) Squashed oocytes were analyzed by immunostaining with anti-FLAG antibodies (red), anti-SYCP3 antiserum (green), and nuclear counterstaining was performed with DAPI (blue). Nu, nucleus; Cy, cytoplasm. Bar, 20 μm.

has provided a cohort of candidate meiotic genes.[35] The authors of this report performed expression profiles of male and female gonads from mouse and human, and compared these patterns to detect conserved co-expression networks. Interestingly, MLZ-611 has a co-expression link with *Sycp3*, and MLZ-638 has co-expression links with *Smc1b*, *Sycp3*, *Hormad2*, and *Dmc1* across mouse and human systems. This indicates that MLZ-611 and MLZ-638 have potential functional connections with well-known meiotic genes in human.

Our final goal in the present study was to identify genes that may have a role in human infertility or RPL. Genes in our candidate lists that are verified as meiotic genes will be further assessed in the future using high-throughput mutational analysis involving targeted next-generation sequencing of genomic DNA from patients with reproductive problems. Recently, exome sequencing has been widely applied to the identification of causative mutations for human diseases.[36–38] However, this approach has been mainly limited to analyses of rare diseases because it is still too costly at present, to screen for mutations responsible for common diseases such as infertility or RPL in this way. Reducing the number of genes to be analyzed, as well as employing simultaneous analysis of multiple samples using barcoded primers assigned to each patient,[39] will allow the genome analyses to be conducted more cost-effectively and more rapidly.

ACKNOWLEDGEMENTS

We thank Dr Hiroki Kano and Ms Chiaki Shimizu for technical assistance. These studies were supported by a grant-in-aid for Scientific Research from the Ministry of Education, Culture, Sports, Science, and Technology of Japan, and a grant from the Hori Information Science Promotion Foundation.

1 Smith, S., Pfeifer, S. M. & Collins, J. A. Diagnosis and management of female infertility. *JAMA* **290,** 1767–1770 (2003).
2 Sierra, S. & Stephenson, M. Genetics of recurrent pregnancy loss. *Semin. Reprod. Med.* **24,** 17–24 (2006).
3 Stephenson, M. D. Frequency of factors associated with habitual abortion in 197 couples. *Fertil. Steril.* **66,** 24–29 (1996).
4 Li, T. C., Makris, M., Tomsu, M., Tuckerman, E. & Laird, S. Recurrent miscarriage: aetiology, management and prognosis. *Hum. Reprod. Update* **8,** 463–481 (2002).
5 Matzuk, M. M. & Lamb, D. J. The biology of infertility: research advances and clinical challenges. *Nat. Med.* **14,** 1197–1213 (2008).
6 Miyamoto, T., Hasuike, S., Yogev, L., Maduro, M. R., Ishikawa, M., Westphal, H. *et al.* Azoospermia in patients heterozygous for a mutation in SYCP3. *Lancet* **362,** 1714–1719 (2003).
7 Christensen, G. L., Ivanov, I. P., Atkins, J. F., Mielnik, A., Schlegel, P. N. & Carrell, D. T. Screening the SPO11 and EIF5A2 genes in a population of infertile men. *Fertil. Steril.* **84,** 758–760 (2005).
8 Mandon-Pépin, B., Touraine, P., Kuttenn, F., Derbois, C., Rouxel, A., Matsuda, F. *et al.* Genetic investigation of four meiotic genes in women with premature ovarian failure. *Eur. J. Endocrinol.* **158,** 107–115 (2008).
9 Bolor, H., Mori, T., Nishiyama, S., Ito, Y., Hosoba, E., Inagaki, H. *et al.* Mutations of the SYCP3 gene in women with recurrent pregnancy loss. *Am. J. Hum. Genet.* **84,** 14–20 (2009).
10 Cohen, P. E., Pollack, S. E. & Pollard, J. W. Genetic analysis of chromosome pairing, recombination, and cell cycle control during first meiotic prophase in mammals. *Endocr. Rev.* **27,** 398–426 (2006).
11 Hassold, T., Hall, H. & Hunt, P. The origin of human aneuploidy: where we have been, where we are going. *Hum. Mol. Genet.* **16,** R203–R208 (2007).
12 Kurahashi, H., Bolor, H., Kato, T., Kogo, H., Tsutsumi, M., Inagaki, H. *et al.* Recent advance in our understanding of the molecular nature of chromosomal abnormalities. *J. Hum. Genet.* **54,** 253–260 (2009).
13 Kogo, H., Tsutsumi, M., Ohye, T., Inagaki, H., Abe, T. & Kurahashi, H. HORMAD1-dependent checkpoint/surveillance mechanism eliminates asynaptic oocytes. *Genes Cells* **17,** 439–454 (2012).
14 Kogo, H., Kowa-Sugiyama, H., Yamada, K., Bolor, H., Tsutsumi, M., Ohye, T. *et al.* Screening of genes involved in chromosome segregation during meiosis I: toward the identification of genes responsible for infertility in humans. *J. Hum. Genet.* **55,** 293–299 (2010).
15 Tsutsumi, M., Kogo, H., Kowa-Sugiyama, H., Inagaki, H., Ohye, T. & Kurahashi, H. Characterization of a novel mouse gene encoding an SYCP3-like protein that relocalizes from the XY body to the nucleolus during prophase of male meiosis I. *Biol. Reprod* **85,** 165–171 (2011).
16 Kawabata, I., Umeda, T., Yamamoto, K. & Okabe, S. Electroporation-mediated gene transfer system applied to cultured CNS neurons. *Neuroreport* **15,** 971–975 (2004).
17 Nakamura, Y., Yamamoto, M. & Matsui, Y. Introduction and expression of foreign genes in cultured mouse embryonic gonads by electroporation. *Reprod. Fertil. Dev.* **14,** 259–265 (2002).
18 Page, J., Suja, J. A., Santos, J. L. & Rufas, J. S. Squash procedure for protein immunolocalization in meiotic cells. *Chromosome Res.* **6,** 639–642 (1998).
19 Prieto, I., Tease, C., Pezzi, N., Buesa, J. M., Ortega, S., Kremer, L. *et al.* Cohesin component dynamics during meiotic prophase I in mammalian oocytes. *Chromosome Res.* **12,** 197–213 (2004).
20 Hamatani, T., Falco, G., Carter, M. G., Akutsu, H., Stagg, C. A., Sharov, A. A. *et al.* Age-associated alteration of gene expression patterns in mouse oocytes. *Hum. Mol. Genet.* **13,** 2263–2278 (2004).
21 Pan, H., O'brien, M. J., Wigglesworth, K., Eppig, J. J. & Schultz, R. M. Transcript profiling during mouse oocyte development and the effect of gonadotropin priming and development *in vitro*. *Dev. Biol.* **286,** 493–506 (2005).
22 Kocabas, A. M., Crosby, J., Ross, P. J., Otu, H. H., Beyhan, Z., Can, H. *et al.* The transcriptome of human oocytes. *Proc. Natl Acad. Sci. USA* **103,** 14027–14032 (2006).
23 Grøndahl, M. L., Yding Andersen, C., Bogstad, J., Nielsen, F. C., Meinertz, H. & Borup, R. Gene expression profiles of single human mature oocytes in relation to age. *Hum. Reprod.* **25,** 957–968 (2010).
24 Small, C. L., Shima, J. E., Uzumcu, M., Skinner, M. K. & Griswold, M. D. Profiling gene expression during the differentiation and development of the murine embryonic gonad. *Biol. Reprod.* **72,** 492–501 (2005).
25 Gallardo, T. D., John, G. B., Shirley, L., Contreras, C. M., Akbay, E. A., Haynie, J. M. *et al.* Genomewide discovery and classification of candidate ovarian fertility genes in the mouse. *Genetics* **177,** 179–194 (2007).
26 Olesen, C., Nyeng, P., Kalisz, M., Jensen, T. H., Møller, M., Tommerup, N. *et al.* Global gene expression analysis in fetal mouse ovaries with and without meiosis and comparison of selected genes with meiosis in the testis. *Cell. Tissue. Res.* **328,** 207–221 (2007).
27 Houmard, B., Small, C., Yang, L., Naluai-Cecchini, T., Cheng, E., Hassold, T. *et al.* Global gene expression in the human fetal testis and ovary. *Biol. Reprod.* **81,** 438–443 (2009).
28 Hogarth, C. A., Mitchell, D., Evanoff, R., Small, C. & Griswold, M. Identification and expression of potential regulators of the mammalian mitotic-to-meiotic transition. *Biol. Reprod.* **84,** 34–42 (2011).
29 Chu, S., DeRisi, J., Eisen, M., Mulholland, J., Botstein, D., Brown, P. O. *et al.* The transcriptional program of sporulation in budding yeast. *Science* **282,** 699–705 (1998).
30 Primig, M., Williams, R. M., Winzeler, E. A., Tevzadze, G. G., Conway, A. R., Hwang, S. Y. *et al.* The core meiotic transcriptome in budding yeasts. *Nat. Genet.* **26,** 415–423 (2000).
31 Hodges, C. A., Revenkova, E., Jessberger, R., Hassold, T. J. & Hunt, P. A. SMC1beta-deficient female mice provide evidence that cohesins are a missing link in age-related nondisjunction. *Nat. Genet.* **37,** 1351–1355 (2005).
32 Revenkova, E., Herrmann, K., Adelfalk, C. & Jessberger, R. Oocyte cohesin expression restricted to predictyate stages provides full fertility and prevents aneuploidy. *Curr. Biol.* **20,** 1529–1533 (2010).
33 Tachibana-Konwalski, K., Godwin, J., van der Weyden, L., Champion, L., Kudo, N. R., Adams, D. J. *et al.* Rec8-containing cohesin maintains bivalents without turnover during the growing phase of mouse oocytes. *Genes Dev.* **24,** 2505–2516 (2010).
34 Chiang, T., Schultz, R. M. & Lampson, M. A. Meiotic origins of maternal age-related aneuploidy. *Biol. Reprod.* **86,** 1–7 (2012).
35 Su, Y., Li, Y. & Ye, P. Mammalian meiosis is more conserved by sex than by species: conserved co-expression networks of meiotic prophase. *Reproduction* **142,** 675–687 (2011).
36 Bamshad, M. J., Ng, S. B., Bigham, A. W., Tabor, H. K., Emond, M. J., Nickerson, D. A. *et al.* Exome sequencing as a tool for Mendelian disease gene discovery. *Nat. Rev. Genet.* **12,** 745–755 (2011).
37 Ku, C. S., Naidoo, N. & Pawitan, Y. Revisiting Mendelian disorders through exome sequencing. *Hum. Genet.* **129,** 351–370 (2011).
38 Singleton, A. B. Exome sequencing: a transformative technology. *Lancet Neurol.* **10,** 942–946 (2011).
39 Parameswaran, P., Jalili, R., Tao, L., Shokralla, S., Gharizadeh, B., Ronaghi, M. *et al.* A pyrosequencing-tailored nucleotide barcode design unveils opportunities for large-scale sample multiplexing. *Nucleic Acids Res.* **35,** e130 (2007).

Supplementary Information accompanies the paper on Journal of Human Genetics website (http://www.nature.com/jhg)

INTERNAL MEDICINE

□ CASE REPORT □

Anti-Hu-associated Paraneoplastic Encephalomyelitis with Esophageal Small Cell Carcinoma

Toshihiko Shirafuji[1], Fumio Kanda[1], Kenji Sekiguchi[1], Masatsugu Higuchi[1], Hiroshi Yokozaki[2], Keiko Tanaka[3], Hitoshi Takahashi[4] and Tatsushi Toda[1]

Abstract

A 63-year-old woman had anti-Hu-associated paraneoplastic encephalomyelitis (anti-Hu syndrome) caused by esophageal small cell carcinoma (SCC). The patient developed bilateral limbic encephalitis, followed by myelitis, brain stem encephalitis, and autonomic failure. Extensive examination demonstrated SCC of the abdominal lymph nodes that was retrospectively diagnosed as metastasis of esophageal SCC on autopsy. The neuropathological findings were characterized by widespread neuronal loss and gliosis in the central nervous system, as well as patchy loss of myelin and axons in the spinal nerve roots with perivascular lymphocytic infiltration. This is the first detailed clinical and neuropathological report of anti-Hu syndrome caused by esophageal SCC.

Key words: anti-Hu-associated paraneoplastic encephalomyelitis, esophageal small cell carcinoma, multiple lesions

(Intern Med 51: 2423-2427, 2012)
(DOI: 10.2169/internalmedicine.51.6884)

Introduction

Anti-Hu-associated paraneoplastic encephalomyelitis (anti-Hu syndrome) is the most frequent remote effect of cancer, potentially affecting the entire nervous system (1-3). Overall, 61-87% of anti-Hu syndrome cases were associated with pulmonary small cell carcinoma (SCC) (1-5). Only a few cases of anti-Hu syndrome associated with extra-pulmonary SCC have been reported. Anti-Hu syndrome related to SCC of the esophagus is extremely rare (2).

While a common clinical manifestation of the anti-Hu syndrome is sensory neuronopathy, 70% of patients have multiple clinical neurological symptoms and 34% of patients have 3 or more areas of involvement in the nervous system (3) during the course of the disease. There have been only a few reports which discuss multiple regional involvement in central and peripheral nervous systems (6, 7).

A case of anti-Hu syndrome with various paraneoplastic neurological syndromes, including, limbic encephalitis, subacute necrotizing myelitis, and brain stem encephalitis is presented. This is the first detailed clinical and neuropathological report of anti-Hu syndrome with esophageal SCC.

Case Report

A 63-year-old woman who complained of amnesia for one month was referred to our hospital for further examinations. On neurological examination, disorientation and emotional instability were evident. Cortical symptoms, such as aphasia or apraxia, were absent. The Mini-Mental State Examination (MMSE) score was 12/30. The total-intelligence quotient (IQ) was 73 (verbal IQ 79, performance IQ 68) on the Revised Wechsler Adult Intelligence Scale (WAIS-R).

Neurological examination revealed mild weakness of hip flexor bilaterally. Reflexes were increased in bilateral biceps and patellar tendons, and the right Achilles tendon, but were decreased in bilateral triceps and left Achilles tendons. Bilateral plantar responses were indifferent. There was no ataxia or sensory impairment.

[1]Division of Neurology, Kobe University Graduate School of Medicine, Japan, [2]Division of Surgical Pathology, Kobe University Graduate School of Medicine, Japan, [3]Department of Neurology, Kanazawa Medical University, Japan and [4]Department of Pathology, Brain Research Institute, University of Niigata, Japan
Received for publication November 5, 2011; Accepted for publication May 6, 2012
Correspondence to Dr. Toshihiko Shirafuji, tshirafuji@phoenix.kobe-u.ac.jp

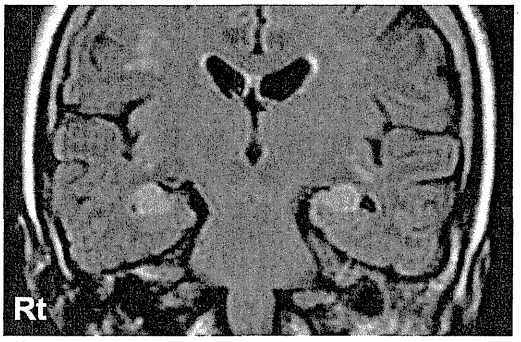

Figure 1. A FLAIR image of the brain MRI on admission shows high signal intensities in bilateral medial temporal lobes including the hippocampus, amygdala, and white matter.

Abdominal CT showed two, 2 to 3 cm diameter, round lymph nodes enhanced with gadolinium. A FLAIR image of the brain showed high signal intensities in the white matter and bilateral medial temporal lobes including the hippocampus and amygdala (Fig. 1). Laboratory tests revealed an increased concentration of serum pro-gastrin-releasing peptide (proGRP) at 69 pg/mL (<45 pg/mL), but serum neuron-specific enolase (NSE) was within normal limits. Cerebrospinal fluid contained 5 white blood cells/μL. Protein and IgG concentrations were 69 mg/dL and 9.4 mg/dL, respectively, and oligoclonal bands were positive in cerebrospinal fluid. Anti-Hu antibody was confirmed in the patient's serum at a titer >2,000. Anti-Yo, -Ri, -CV2, -Tr, -Ma2, and amphiphysin antibodies were negative. Anti-nucleus of the systemic organ antibody, anti-undetermined neuro-histology antibody, anti-ganglioside antibodies, and anti-voltage gated potassium channel antibody were also negative. The patient had HLA B51, one of the HLA B7 supertypes, consistent with a previous report (8).

To obtain a histological diagnosis, biopsy of the abdominal lymph node swelling was performed at 3 weeks. Microscopic examination of the biopsied abdominal lymph node revealed metastasis of SCC. After the biopsy, the patient needed mechanical ventilation due to respiratory muscle weakness. Since the serum proGRP returned to the normal range after the biopsy, chemotherapy was not started.

At week 3, muscular weakness of all extremities progressed, rendering her bedridden at week 5. Neurological examination revealed severe weakness of the upper extremities (grade 2) and the lower extremities (grade 1). Fasciculations were evident and deep tendon reflexes were decreased in all extremities. Bilateral plantar responses were indifferent. The sensory system was normal. Cerebrospinal fluid contained 3 white blood cells/μL. Protein and IgG concentrations were 186 mg/dL and 30.1 mg/dL, respectively, in the cerebrospinal fluid. Nerve conduction studies revealed reduction in amplitude of the compound muscle action potentials in the median nerves with normal motor nerve conduction velocities. The amplitudes of the sensory nerve action potentials and the sensory conduction velocities of the median and sural nerves were normal. Needle electromyography showed many fasciculation potentials with few fibrillation potentials and positive sharp waves (fib/PSW) before the biopsy. Many fib/PSW with a few fasciculation potentials in the right biceps brachii were observed during the progression of the muscular weakness. No waxing or waning phenomenon was observed with repetitive nerve stimulation.

Neither intravenous immunoglobulin infusion therapy (400 mg/kg daily for 5 days) at week 5 nor intravenous methyl-prednisolone pulse therapy (1,000 mg daily for 3 days) at week 10 showed any benefit for her condition.

At weeks 6 to 10, impairment of cranial nerves VI, VII, IX, and X developed and were followed by autonomic malfunctions including orthostatic hypotension, unstable pulse rate, and decreased bowel sounds. The patient developed a succession of bouts of pneumonia at weeks 21, 30, and 40. At week 21, her consciousness level deteriorated to a deep coma. There was flaccid paralysis of all extremities. All tendon reflexes were disappeared. Bilateral plantar responses were indifferent. There was no involuntary movement. The patient died of sepsis 10 months after the onset of the neurological symptoms.

Autopsy findings

A general autopsy was performed about 14 hours after death, at which time the brain weighed 1,280 g. The brain and spinal cord were fixed with 10% formalin, and multiple tissue blocks were embedded in paraffin. Histological examination was performed on 4-μm-thick sections using several stains, including hematoxylin and eosin, Klüver-Barrera, Bodian, and Holtzer. Immunohistochemical examination was also carried out: the spinal cord sections, with the anterior and posterior nerve roots, and esophageal cancer tissue sections were immunostained using an antibody against phosphorylated neurofilament (SMI-31, Sternberger Monoclonals, Bethesda, MD, USA).

Macroscopic findings

A general autopsy revealed a tumor arising in the middle part of the esophagus (Fig. 2) with metastasis to the regional para-aortic lymph nodes, which was later shown histopathologically to be SCC; the tumor cells were positive for cytokeratin, CD56 and synaptophysin (data not shown). There was no lymph node involvement other than the regional lymph nodes, consistent with the limited disease (LD).

The brain, including brain stem, cerebellum, and spinal cord, was almost entirely soft and pale. The cerebral cortex showed thinning and pale-brownish discoloration, being more marked in the lateral temporal lobe. The subcortical white matter also showed a coarse granular appearance.

Microscopic findings

Histopathological examination of the brain and spinal cord revealed apparent neuronal loss and gliosis in almost the entire cerebral cortex, brainstem lower motor neuron nuclei [severe in the oculomotor (III) and hypoglossal (XII)

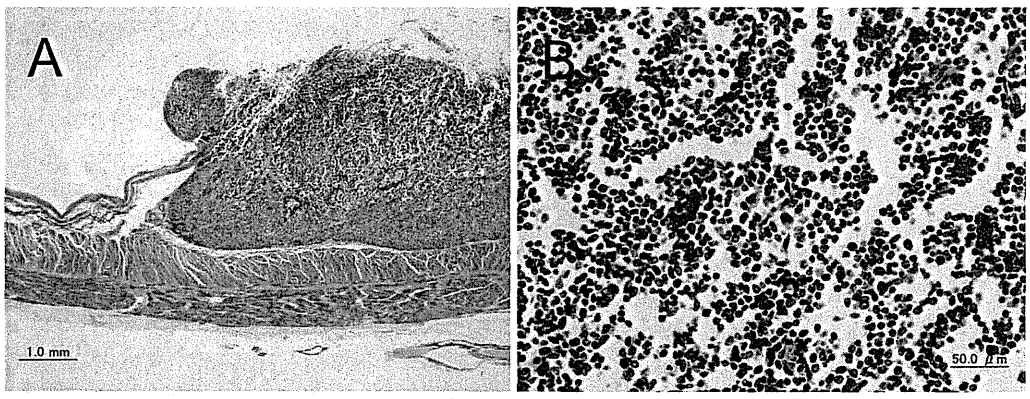

Figure 2. A tumor in the middle region of the esophagus (A), consisting of small cancer cells (B) (Hematoxylin and Eosin staining).

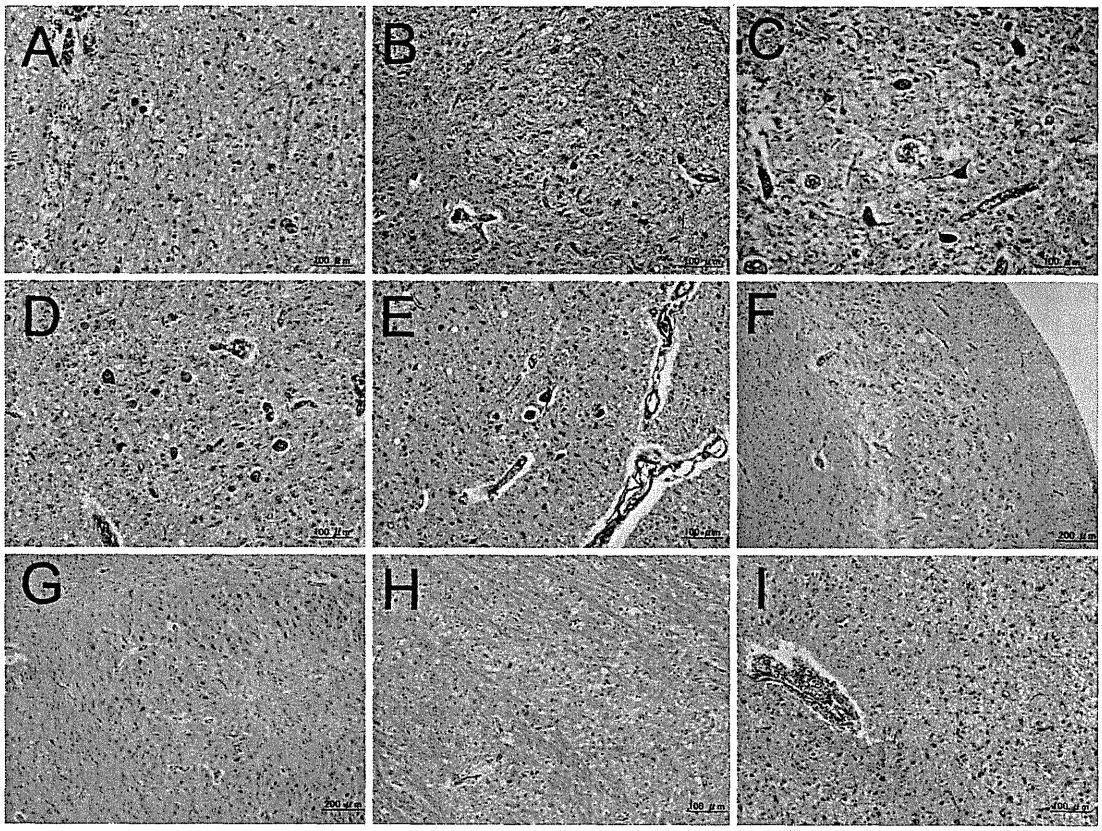

Figure 3. Neuronal loss and gliosis in the lower motor neuron nuclei: severe in the oculomotor (III) (A) and hypoglossal (XII) (B) nuclei; moderate in the motor nuclei of the trigeminal (V) (C) and facial (VII) nerves (D); and mild in the nucleus ambiguus (E). In the hippocampus, CA1-2 and the subiculum (F) are relatively preserved. However, severe neuronal loss and gliosis are evident in CA3-4 (G). Moderate neuronal loss is observed in the putamen (H) and thalamus (I).

nuclei; moderate in the motor nuclei of the trigeminal (V) and facial (VII) nerves; and mild in the nucleus ambiguus], hippocampus (severe in CA3-4, relatively preserved in CA1-2 and the subiculum), parahippocampal gyrus (moderate), amygdala (severe in the medial part), caudate nucleus (moderate), putamen (moderate), thalamus (moderate), brainstem reticular formation including the raphe nucleus (severe), gracile and cuneate nuclei (severe), inferior olivary nucleus (severe), and spinal gray matter (severe in the anterior horn, relatively preserved in the posterior horn and intermediolateral nucleus) (Fig. 3, Fig. 4B, and Table). There was diffuse myelin pallor in the cerebral white matter. Diffuse myelin pallor with macrophage infiltration was also evident in the brainstem (central tegmental tract and medial leminiscus) and spinal cord (Fig. 4A). There was patchy myelin pallor in both spinal anterior and posterior nerve roots (Fig. 4C).

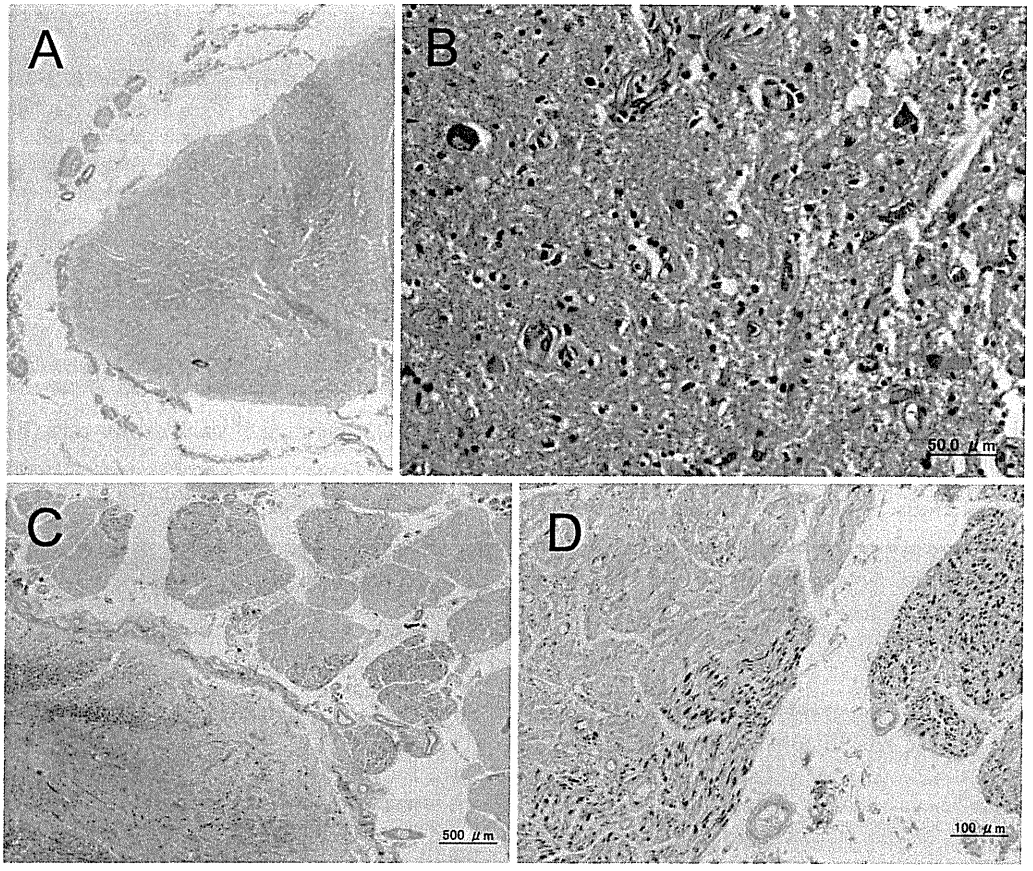

Figure 4. Diffuse myelin pallor is evident in the spinal white matter, including the lateral corticospinal tract (A). Severe neuronal loss and gliosis is evident in the lumbar anterior horn (B). Myelin pallor is evident in the nerve roots (C). SMI-31 immunostaining demonstrates patchy loss of myelinated axons (D).

Table. Degree of Neuronal Loss in the Central Nervous System

Degree of neuronal loss	Site
Severe	occulomotor nuclei, hypoglossal nuclei, hippocampus (CA3-4), amygdala, raphe nucleus, gracile and cuneate nuclei, inferior olivary nucleus, anterior horn, Purkinje cell
Moderate	nuclei of the trigeminal and facial nerve , hippocampus (CA1-2 and subiculum), parahippocampal gyrus, caudate nucleus, putamen, thalamus, posterior horn and intermediolateral nucleus, cerebellar dentate nucleus
Mild	nucleus ambiguus

Immunostaining with SMI31, a marker for axon, also showed patchy axonal damage (Fig. 4D). Purkinje cell loss and Bergmann's gliosis were evident in the cortex, being more marked in the superior part of the vermis. The cerebellar dentate nucleus was relatively well preserved. Occasional perivascular and intraparenchymal lymphocytic infiltration was seen throughout the entire affected regions. A few microglial nodule- and neuronophagia-like lesions were also seen in the affected brainstem and spinal gray matter.

Discussion

The present case was characteristic in its combination of symptoms of mental deterioration, upper and lower motor neuron disturbance, and various autonomic system failures with rapid progression. Extensive work-up for the origin of the malignancy was negative, and an autopsy first revealed the esophageal SCC. We concluded that the neurological deficit was caused by a paraneoplastic etiology because there was no tumor invasion in the nervous system. Moreover, since anti-Hu antibody was detected in her serum, this patient was diagnosed with anti-Hu syndrome.

The autopsy examination showed severe disintegration in the major part of the brain in the present patient. It was difficult to determine whether the damage originated from the hypoxia due to the pneumonia or the anti-Hu syndrome. Despite the softness of the brain, global ischemia or hypoxia could be excluded because the vulnerable regions for hypoxia including the basal ganglia, Ammon's horn, tegmentum, substantia nigra, and calcarine, were relatively preserved microscopically. Moreover, whole layer involvement, not laminar necrosis, was evident throughout the entire cortex. These findings suggested that the broad damage of the

nervous system was due not to hypoxia but to the anti-Hu syndrome.

The characteristic pathological findings of anti-Hu syndrome with pulmonary SCC are neuronal loss with reactive gliosis, microglial proliferation, and perivascular lymphocytic cuffing (9). In the present case, neuronal loss with gliosis and lymphocytic infiltration in the brain including brain stem, cerebellum, and spinal cord was confirmed. It was indicated that neuropathological features in anti-Hu paraneoplastic neurological syndromes caused by esophageal SCC were similar to those by pulmonary SCC.

During the course of the anti-Hu syndrome, multiple areas of the nervous system became involved in 70% of the patients (2, 3). However, only a limited number of neuropathological studies of anti-Hu syndrome with multiple areas involvement has been reported (6, 7). Multiple neuropathological lesions correlated with the multiple clinical symptoms were confirmed in the present case. Neurological complications, mostly ventilatory failure and dysautonomia, appear to be the most common causes of death (3), as in the present case.

Because the symptoms of anti-Hu syndrome tend to occur before tumor detection, it is important to know the candidate organs for the primary site. Esophageal SCC is one of the common sites of extrapulmonary SCC (10). However, there have been reports of a few paraneoplastic syndrome cases with esophageal carcinoma (11-15). Moreover, anti-Hu syndrome with esophageal carcinoma was reported in only 1 of 200 patients without pathological study (2). Therefore, to the best of our knowledge, this is the first detailed report of anti-Hu syndrome related to esophageal SCC. The present case showed that esophageal SCC could be a cause of the anti-Hu syndrome. It is necessary to consider esophageal SCC as a candidate primary lesion responsible for anti-Hu syndrome.

The authors state that they have no Conflict of Interest (COI).

Acknowledgement

The authors would like to thank Dr. Osamu Watanabe in Kagoshima University for measurement of anti-VGKC antibody.

References

1. Sillevis Smitt P, Grefkens J, de Leeuw B, et al. Survival and outcome in 73 anti-Hu positive patients with paraneoplastic encephalomyelitis/sensory neuronopathy. J Neurol **249**: 745-753, 2002.
2. Graus F, Keime-Guibert F, Reñe R, et al. Anti-Hu-associated paraneoplastic encephalomyelitis: analysis of 200 patients. Brain **124**: 1138-1148, 2001.
3. Dalmau J, Graus F, Rosenblum MK, Posner JB. Anti-Hu--associated paraneoplastic encephalomyelitis/sensory neuronopathy. A clinical study of 71 patients. Medicine (Baltimore) **71**: 59-72, 1992.
4. Remick SC, Ruckdeschel JC. Extrapulmonary and pulmonary small-cell carcinoma: tumor biology, therapy, and outcome. Med Pediatr Oncol **20**: 89-99, 1992.
5. Levenson RM Jr., Ihde DC, Matthews MJ, et al. Small cell carcinoma presenting as an extrapulmonary neoplasm: sites of origin and response to chemotherapy. J Natl Cancer Inst **67**: 607-612, 1981.
6. Heidenreich F, Schober R, Brinck U, Hartung HP. Multiple paraneoplastic syndromes in a patient with antibodies to neuronal nucleoproteins (anti-Hu). J Neurol **242**: 210-216, 1995.
7. Yamada M, Inaba A, Yamawaki M, et al. Paraneoplastic encephalo-myelo-ganglionitis: cellular binding sites of the antineuronal antibody. Acta Neuropathol **88**: 85-92, 1994.
8. Tanaka M, Maruyama Y, Sugie M, Motizuki H, Kamakura K, Tanaka K. Cytotoxic T cell activity against peptides of Hu protein in anti-Hu syndrome. J Neurol Sci **201**: 9-12, 2002.
9. Farrugia ME, Conway R, Simpson DJ, Kurian KM. Paraneoplastic limbic encephalitis. Clin Neurol Neurosurg **107**: 128-131, 2005.
10. Kim KO, Lee HY, Chun SH, Shin SJ, et al. Clinical overview of extrapulmonary small cell carcinoma. J Korean Med Sci **21**: 833-837, 2006.
11. Cox PM, Vazir MH, Petty RK, Law S, Dhillon AP. Cerebellar cortical degeneration in association with small-cell carcinoma of the oesophagus. Neuropathol Appl Neurobiol **15**: 175-183, 1989.
12. Gritzman MC, Fritz VU, Perkins S, Kaplan CL. Motor neuron disease associated with carcinoma. A report of 2 cases. S Afr Med J **63**: 288-291, 1983.
13. Sutton IJ, Fursdon Davis CJ, Esiri MM, Hughes S, Amyes ER, Vincent A. Anti-Yo antibodies and cerebellar degeneration in a man with adenocarcinoma of the esophagus. Ann Neurol **49**: 253-257, 2001.
14. Dodgson MC, Hoffman HL. Sensory neuropathy associated with carcinoma of the esophagus; report of a case. Ann Intern Med **38**: 130-135, 1953.
15. Khealani BA, Qureshi R, Wasay M. Motor neuronopathy associated with adenocarcinoma of esophagus. J Pak Med Assoc **54**: 165-166, 2004.

MYOSITIS WITH ANTIMITOCHONDRIAL ANTIBODIES DIAGNOSED BY RECTUS ABDOMINIS MUSCLE BIOPSY

TAKESHI UENAKA, MD,[1] HISATOMO KOWA, MD, PhD,[1] KENJI SEKIGUCHI, MD, PhD,[1] KAKUYA NAGATA, MD,[1] YOSHIHISA OHTSUKA, MD,[1] FUMIO KANDA, MD, PhD,[1] and TATSUSHI TODA, MD, PhD[1]

Division of Neurology, Kobe University Graduate School of Medicine and Kobe University Hospital, 7-5-2 Kusunoki-cho, Chuo-Ku, Kobe, Hyogo 650-0017, Japan

Accepted 14 November 2012

ABSTRACT: *Introduction:* Antimitochondrial antibodies are autoantibodies detected in 90% of primary biliary cirrhosis (PBC) patients. Some PBC cases are complicated by myositis, which is difficult to confirm due to minimal histological evidence of inflammation in limb muscles. *Methods:* Our aim was to determine the extent of inflammatory changes in a truncal muscle biopsy specimen from a PBC patient. *Results:* A 48-year-old woman with a 5-year history of atrial fibrillation and chronic heart failure was evaluated for elevated serum creatine kinase level. Antimitochondrial M2 antibodies were detected, and PBC was diagnosed. A biceps brachii biopsy specimen showed mild, non-specific myogenic changes; a second biopsy was performed on the rectus abdominis muscle, which showed typical inflammatory changes. Myositis with antimitochondrial M2 antibodies was confirmed. *Conclusions:* In myositis patients with antimitochondrial M2 antibodies, muscles of the extremities are involved to a lesser extent. Radiological and histological examination focusing on truncal muscles, including a biopsy, is important.

Muscle Nerve **47**:766–768, 2013

Primary biliary cirrhosis (PBC) is known to be associated with a rare complication of myositis. Recently, a small number of patients with myositis and PBC have been reported in the literature, with clinical characteristics that differ from those of classical polymyositis (e.g., some reports showed only sparse infiltrates in biopsy specimens from the extremities[1–4] and more severe heart/respiratory failure[5,6]). In this report, we describe a 48-year-old woman with mild muscle weakness and severe heart failure who was diagnosed by histological study of a rectus abdominis muscle biopsy specimen.

CASE REPORT

In August 2006, a 48-year-old Japanese woman visited a local hospital complaining of palpitation and dyspnea on exertion. She was diagnosed with atrial fibrillation that recovered to normal sinus rhythm with cardioversion. Her serum creatine kinase concentration was elevated at that time (600–1000 IU/L). In July 2007, she was admitted for catheter ablation for relapse of atrial fibrillation. Six months later she was readmitted for congestive heart failure. In 2010, the patient felt increasing fatigue after standing and lifting bags. In December 2010, she was admitted again for treatment of an exacerbation of chronic heart failure. After further examination, she was diagnosed with cardiomyopathy of unknown etiology (the coronary angiogram was normal, and a biopsy specimen from the myocardium showed non-specific fibrosis). Systemic myopathy was suspected as the potential cause of the cardiomyopathy, and the patient was referred to our department for intensive examination and treatment.

Physical examination indicated irregular heart sounds without murmur. The patient's abdomen was flat and mildly firm without any tenderness. Neurological examination revealed mild weakness in proximal limb and trunk muscles (grade 4/5 on manual muscle testing), with slightly reduced deep tendon reflexes. She did not complain of any problems with standing, routine gait, or autonomic failure. Warfarin, furosemide, spironolactone, sodium ferrous citrate, and candesartan were prescribed.

Laboratory findings were as follows: white blood cell count 4000 cells/mm^3; hemoglobin 9.2 g/dl; platelets 79 × 10^3 platelets/mm^3; total bilirubin 1.2 mg/dl; aspartate aminotransferase 37 IU/L; alanine aminotransferase 33 IU/L; alkaline phosphatase 790 IU/L; C-reactive protein 0.5 mg/dl, and erythrocyte sedimentation rate 62 mm/h. Serum creatine kinase and aldolase levels were 351 IU/L (normal 46–168 IU/L) and 8.9 IU/L (normal 2.2–5.5 IU/L), respectively, and brain natriuretic peptide levels were elevated (121.04 pg/ml). Vitamin B_{12} levels were low (192 pg/ml). Results were negative for antinuclear antibodies, anti–U1-ribonucleoprotein, anti–SS-A, anti–SS-B, and anti–Jo-1. The patient had positive antimitochondrial antibodies at a titer of >1:80 and antibodies to mitochondrial M2 at titers of 137.3 IU/L (normal <7.0 IU/L). Arterial blood gas analysis showed mild hypercapnea of 46.8 mm Hg (normal 32–46

Abbreviations: FEV_1, forced expiratory volume in 1 second; PBC, primary biliary cirrhosis; VC, vital capacity

Key words: antimitochondrial antibody; anti-M2 antibody; cardiac complication; polymyositis; primary biliary cirrhosis

Correspondence to: T. Uenaka; e-mail: onlytan@med.kobe-u.ac.jp

Published online 21 November 2012 in Wiley Online Library (wileyonlinelibrary.com). DOI 10.1002/mus.23730

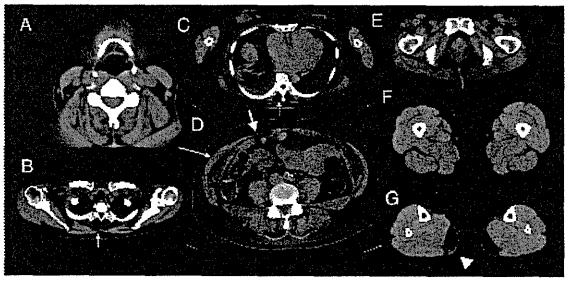

FIGURE 1. Limb and abdominal computed tomography shows bilateral fatty displacement of the rectus abdominis (short, thick arrow), abdominal obliques (long, thin arrow), paravertebral (short, thin arrow), and gastrocnemius (arrow head) muscles. Slices are at the levels of thyroid cartilage **(A)**, acromion **(B)**, mid-thoracic **(C)**, hypogastrium **(D)**, pubic symphysis **(E)**, mid-thigh **(F)**, and upper third of the leg **(G)**, respectively.

mm Hg; i.e., 4.27–6.00 kPa), and electrocardiography showed atrial fibrillation. Furthermore, chest radiography and computed tomography indicated cardiomegaly and congestion in both lungs, but there was no interstitial pulmonary fibrosis.

Echocardiography showed dilation of the left atrium, hypokinesis of the posterior–inferior region beyond 1 coronary territory, low ejection fraction (44%), and mild pulmonary hypertension (44 mm Hg). A respiratory function test showed reduced vital capacity (1520 ml, VC = 49.7%) and normal forced expiratory volume in 1 second (FEV_1 = 78.3%). Abdominal ultrasonography showed mild hepatomegaly with splenomegaly, and the patient was diagnosed clinically to have primary biliary cirrhosis (PBC) based on elevated hepatic enzymes and anti-M2 antibodies. Splenomegaly was probably due to PBC. She did not accept a liver biopsy. Needle electromyography of proximal muscles showed mild fibrillation potentials and positive sharp waves. Abdominal and limb computed tomography showed fatty replacement of bilateral rectus abdominis, abdominal oblique, paravertebral, and gastrocnemius muscles (Fig. 1).

Histological study of a muscle biopsy specimen taken from the patient's left biceps brachii showed near-normal morphology, with no necrosis or regenerative fibers and few mononuclear-cell infiltrations. Subsequently, an additional biopsy specimen was taken from the rectus abdominis muscle and showed necrotic and regenerating fibers with 1 large infiltrate of CD4-positive mononuclear cells and fat (Fig. 2).

We started treatment with prednisolone (1 mg/kg/day) and ursodeoxycholic acid (600 mg/day). Subsequently, the patient had marked improvement in dyspnea on exertion, serum muscle enzyme levels, and ejection fraction (60% 1 month after treatment). Two months later, her VC also improved (2150 ml, VC = 70.3%). Her anemia and low platelet count improved after intravenous vitamin B_{12} supplementation, suggesting that her pancytopenia was due to vitamin B_{12} deficiency.

DISCUSSION

Maeda *et al.*[7] reported that myositis with anti-M2 antibodies accounts for 10% of all inflammatory myopathy cases. Anti-M2 antibody-related myositis exhibits specific features, such as a chronic clinical course, cardiomyopathy with arrhythmia and left ventricular systolic dysfunction, muscle atrophy primarily in truncal muscles, improved symptoms with prednisolone administration (monophasic course), and arrhythmia that worsens when left untreated. Our patient showed similar characteristics of myositis with anti-M2 antibodies, including moderate congestive heart failure and refractory arrhythmia, and the time period from onset of arrhythmia to diagnosis of myositis with anti-M2 antibodies was 5 years.[7]

In a case of inflammatory myopathy, histological confirmation of the diagnosis is essential before initiating immunosuppressive treatment with glucocorticoids due to the possibility of associated side effects. The muscle biopsy specimen typically shows a mixture of necrosis and regeneration of muscle fibers with lymphocytic infiltration. Although inflammatory myopathies are systemic disorders, pathological processes develop heterogeneously. In some cases, typical findings of myositis are not seen in muscle biopsy specimens due to sampling error. Consequently, biopsy site localization is important to obtain useful information for histological diagnosis.

In patients with myositis with anti-M2 antibodies, abnormal clinical and pathological findings are often more evident in truncal muscles than in the extremities. In some reports,[2,4] biopsy of the biceps/quadriceps did not show any characteristics of active inflammatory changes; the investigators suspected that chronicity of the condition (i.e., the biopsy was performed too late) and/or immunosuppressive therapy affected the findings. In our patient the first muscle biopsy performed on her

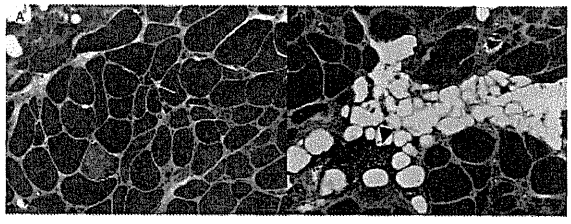

FIGURE 2. (A, B) Rectus abdominis muscle biopsy shows necrotic (black arrow) and regenerating fibers (yellow arrow) with endomysial infiltration (black arrow head) of mononuclear cells and fat. There were many fibers with internal nuclei. (hematoxylin and eosin stain; original magnification ×200). [Color figure can be viewed in the online issue, which is available at wileyonlinelibrary.com.]

left biceps brachii provided no useful diagnostic information. In myositis patients with anti-M2 antibodies, frequent truncal muscle involvement by has been reported, as demonstrated by computed tomography.[7] In addition, the fatty changes in her gastrocnemius muscles were so extensive that we could not expect to find specific inflammatory changes. Thus, we performed the second muscle biopsy on the rectus abdominis and obtained characteristic findings that confirmed our diagnosis. Immunotherapy using glucocorticoids immediately improved the patient's clinical symptoms and laboratory data. Her cardiac and respiratory failure also improved promptly with treatment.

Myositis with anti-M2 antibodies is difficult to diagnose because of its complex clinical features and unusual distribution of inflammatory changes in the affected muscles. For accurate diagnosis, it is essential to obtain an appropriate sample for histological assessment. After myositis with anti-M2 antibodies is confirmed, treatment with glucocorticoids is effective to address not only muscle symptoms but also cardiac complications.

The authors thank Dr. Meiko Hashimoto Maeda and Dr. Jun Shimizu (Department of Neurology, University of Tokyo) for their valuable suggestions, information, and discussion. We also thank Chiyomi Ito and Dr. Motoi Kanagawa for excellent technical assistance.

REFERENCES

1. Sato T, Kato J, Sato Y, Iyama S, Takada K, Oku T, et al. A case of primary biliary cirrhosis with HLA-DR 8 complicated by polymyositis. Liver 2003;44:455–459.
2. Saitoh S, Yamada S, Takagi H, Abe T, Takezawa J, Nagamine T, et al. A male autopsy case of primary biliary cirrhosis associated with polymyositis and congestive cardiomyopathy. Nihon Shokakibyo Gakkai Zasshi 1988;85:287–291.
3. Kurihara Y, Shishido T, Oku K, Takamatsu M, Ishiguro H, Suzuki A, et al. Polymyositis associated with autoimmune hepatitis, primary biliary cirrhosis, and autoimmune thrombocytopenic purpura. Mod Rheumatol 2011;21:325–329.
4. Migueletto BC, Neto AE, Domingues EZ, Neves de Castro PP, Stocker H, Marie SK, et al. Primary biliary cirrhosis and myopathy: an uncommon association. Rev Hosp Clin Fac Med Sao Paulo 1999;54:165–168.
5. Varga J, Heiman-Patterson T, Munoz S, Love LA. Myopathy with mitochondrial alterations in patients with primary biliary cirrhosis and antimitochondrial antibodies. Arthritis Rheum 1993;36:1468–1475.
6. Matsui K, Aizawa Y, Inoue K, Yaguchi H, Toda G. Polymyositis with marked paravertebral muscle atrophy in patients with primary biliary cirrhosis. Rinsho Shinkeigaku 2000;40:694–700.
7. Maeda MH, Tsuji S, Shimizu J. Inflammatory myopathies associated with anti-mitochondrial antibodies. Brain 2012;135:1767–1777.

THE FROMENT–RAUBER NERVE: A CASE REPORT AND REVIEW

JOSEPH H. KAMERATH, MD,[1] DAVID K. EPSTEIN, MD,[2] and KEVIN F. FITZPATRICK, MD[3]

[1] Department of Physical Medicine and Rehabilitation, Walter Reed National Military Medical Center, Bethesda, Maryland, USA
[2] Department of Neurology, Naval Medical Center Portsmouth, Portsmouth, Virginia, USA
[3] Mount Vernon Rehabilitation Medicine Associates, Alexandria, Virginia, USA

Accepted 27 November 2012

ABSTRACT: *Introduction:* The Froment–Rauber nerve is a rarely described anomalous nerve arising from 1 of the terminal branches of the radial nerve that provides innervation to intrinsic hand muscles. We describe a 26-year-old man who had a traumatic radial nerve injury that resulted in first dorsal interosseous muscle wasting. He presented to our clinic 2.5 years post-injury, after having had unnecessarily undergone surgical exploration of the ulnar nerve. *Methods:* The patient's history, clinical examination, and multiple electrodiagnostic tests were reviewed. *Results:* All findings were consistent with a diagnosis of anomalous innervation via a Froment–Rauber nerve. *Conclusions:* Understanding this rare phenomenon may aid in diagnosing confusing clinical cases and prevent unnecessary procedures.

Muscle Nerve **47**:768–771, 2013

Abbreviations: AIN, anterior interosseous nerve; CMAP, compound motor action potential; EDx, electrodiagnostic examination; FDI, first dorsal interosseous muscle; PIN, posterior interosseous nerve; SRN, superficial radial nerve

Disclosure: The authors thank Eleni H. Aldridge and Thomas R. Piers for their artwork. The views expressed in this article are those of the authors and do not necessary reflect the official policy or position of the Department of the Army, Department of the Navy, Department of Defense, nor the U.S. Government.
Key words: anomalous innervation; first dorsal interosseous; Froment–Rauber nerve; posterior interosseous neurectomy; superficial radial nerve
Correspondence to: J.H. Kamerath, 3615 Holiday Drive SE, Olympia, WA 98501; e-mail: jkamerath@gmail.com

Published online 29 November 2012 in Wiley Online Library (wileyonlinelibrary.com). DOI 10.1002/mus.23741

Variations in innervation of the intrinsic hand muscles are well known and include the Martin–Gruber and Riche–Cannieu anastomoses. Understanding these variations is important for proper diagnosis and treatment. The Froment–Rauber nerve is a lesser known variant in intrinsic hand innervation. It is a rarely described anomalous branch of either the posterior interosseous nerve (PIN) or superficial radial nerve (SRN) that provides innervation to intrinsic hand muscles, typically the first dorsal interosseous (FDI), but other muscles may also receive innervation from this anomaly.[1]

CASE REPORT

We describe a 26-year-old, right-hand-dominant man who had a gunshot wound to the right arm resulting in a humeral fracture. He underwent surgical exploration and fracture repair. The operative report was not available, and there was no record of nerve injury. He was noted to have a wrist drop and was referred for electrodiagnostic examination (EDx) 3 months after his injury.

BRAIN and NERVE 65(3)：227-234，2013

特 集 次世代シーケンサーによる神経変性疾患の解析と展望

パーソナルゲノム研究と神経疾患 — overview

Personal Genome Research and Neurological Diseases: Overview

戸 田 達 史*

Tatsushi Toda*

Abstract

Neurological diseases include those caused by a single defective gene, e.g., Huntington's disease, other polyglutamine diseases, and muscular dystrophies, and those that are mostly sporadic but rarely show Mendelian inheritance in some families, e.g., Alzheimer's disease, Parkinson's disease, amyotrophic lateral sclerosis, and epilepsy. The latter diseases are considered polygenic disorders. Both sporadic and Mendelian cases of these diseases are believed to share some common pathological mechanisms. Since the detection of causal genes for the Mendelian cases, studies have been initiated on disease pathology. SNPs and rare gene variants play important roles in common neurological diseases. From a technological perspective, next-generation sequencers have become widely available and have contributed to the advancement of research based on individual genome sequences (personal genome). This paper presents an overview, as well as a historical context, of the contribution of personal genome research to neurological disease studies.

Key words：GWAS, rare variant, next-generation sequencer, neurological disease, personal genome

はじめに

神経疾患には，ハンチントン病など各種のポリグルタミン病，各種の筋ジストロフィーなどのように単一遺伝子の異常によるものと，アルツハイマー病，パーキンソン病，筋萎縮性側索硬化症，てんかんなどのように，患者の大部分は孤発性だが一部にメンデル遺伝をとる家系が存在するものがある。後者は生活習慣病などと同様に多因子遺伝性疾患と考えられている。後者のうち孤発性のものもメンデル遺伝性のものも，一部共通の発症メカニズムが存在していると考えられ，このうちメンデル遺伝を示すものは原因遺伝子が明らかにされており，それらを切り口にして病態解明が進んでいる。一方，テクノロジーの進展はめざましく，次世代シーケンサーが実用化され個々のゲノム配列（パーソナルゲノム）をもとにした研究が展開されるようになってきている。本稿ではパーソナルゲノム研究が神経疾患解明に与えるものについて歴史的な経緯も含めて述べる。

Ⅰ．単一遺伝性神経変性疾患原因遺伝子の同定と共通の分子機構

1990年代以降ポジショナルクローニングによって，単一遺伝性疾患としての遺伝性神経変性疾患の病因遺伝子の解明は急速に進んだ。単一遺伝子による遺伝性疾患に関しては，染色体上に存在する遺伝マーカーを用いた連鎖解析により原因遺伝子の存在場所が決定され，それが狭められ，続いてその領域に存在する遺伝子で患者家系の変異解析が行われる手法で，多数の原因遺伝子が同定されてきた。この種の連鎖解析法では遺伝形式，遺伝子頻度，浸透率などのパラメーターを必要とするのでパラメトリック連鎖解析と呼ばれる。

遺伝学上の歴史的なものとしてデュシェンヌ型筋ジストロフィー原因蛋白ジストロフィン，ハンチントン病原因蛋白ハンチンチンなどが挙げられるが，他に，家族性

* 神戸大学大学院医学研究科神経内科学〔〒650-0017 兵庫県神戸市中央区楠町7-5-1〕Division of Neurology, Kobe University Graduate School of Medicine, 7-5-1 Kusunoki-cho, Chuo-ku, Kobe, Hyogo 650-0017, Japan

1881-6096/13/¥500/論文/JCOPY

アルツハイマー病，前頭側頭型認知症，家族性パーキンソン病，脊髄小脳変性症，筋萎縮性側索硬化症など枚挙にいとまがない。ハンチントン病原因遺伝子などからCAGリピート病の概念も生まれ，さらに各種の脊髄小脳変性症原因遺伝子も同定されていった。CAGはグルタミンをコードするため，翻訳領域内にみられるものはポリグルタミン病とも総称される。筆者らも日本に特異的に多い福山型筋ジストロフィーの原因遺伝子フクチンを同定し，本症が約100世代前の1人の祖先に起きたレトロトランスポゾン変異が広がった初めての疾患であることを見出した。

単一遺伝性疾患については，数多くの病因遺伝子が同定されたことを受けて，研究の焦点は，その病態機序を解明することに移ってきており，原因療法の開発が射程距離に入ったものも多い。ポリグルタミン病では異常伸長ポリグルタミン鎖はコンフォメーション変化を生じた結果，異常伸長鎖特異的な蛋白質間相互作用を獲得したり，あるいは難溶性のポリグルタミン蛋白質凝集体からなる細胞内封入体を形成することが明らかにされている。つまり異常伸長ポリグルタミン鎖の凝集体を形成しやすい性質と細胞毒性とは密接に関連していると考えられている。この現象は，凝集体の構成成分は異なるが，アルツハイマー病，パーキンソン病，筋萎縮性側索硬化症，プリオン病などで共通しており，異常蛋白質の凝集・蓄積が神経変性を引き起こすという共通の分子機構が考えられている。アルツハイマー病ではアミロイドβ凝集阻害をめざした抗体療法[1]，筋ジストロフィーではスプライスを変更させ正常化するアンチセンス療法[2,3]などが試みられており，一部はフェーズIIIに至っているものもある。

II. 多因子疾患とcommon disease-common variants仮説

このような分子遺伝学的研究の成果は，これまでは主として単一遺伝子疾患に対して得られてきていたが，最近は，遺伝性が明確でない，孤発性の疾患に対しても研究が進んでいる。その背景には，ヒトゲノムの多様性が，さまざまな疾患の発症や，薬効，薬剤副作用に関する個人差に関わっているとの考えがあるからである。

生活習慣病で代表されるような多因子疾患については，common disease-common variants仮説に基づいた関連解析（ゲノムワイド関連解析genome-wide association study：GWAS）により，疾患感受性遺伝子の同定をめざした研究が盛んになってきている。Fig. 1にゲノム配列の多様性からみた疾患の発症機構を示す[4]。

単一遺伝子疾患では，特定の遺伝子に病因となる変異が生じることで発症する。このような疾患では，遺伝子変異によるオッズ比は非常に高いことになる。一方，高血圧，糖尿病などの生活習慣病と呼ばれる疾患は，複数の遺伝的な要因（疾患感受性遺伝子）と生活習慣などの環境要因が複合的に作用して発症すると考えられている。このような頻度の高い疾患では，誰もがこのような疾患感受性遺伝子の多型をある程度有している可能性が高いと考えられ，疾患感受性遺伝子に関連する多型による疾患発症のオッズ比は低いものとなる。このように，誰もが持っているような多型性が，疾患の発症に関与するという考え方は，common disease-common variants仮説と呼ばれる（Fig. 1）。

III. ゲノムワイド関連解析（GWAS）

2006年以降，common diseaseの感受性遺伝子の探索研究は新しい段階を迎えた。これをもたらした主な要因は2つの基盤整備である。まず情報基盤として，dbSNPやHapMap計画で代表されるように，ヒトゲノム全域にわたる膨大な多様性情報が集積されてきた。次に技術基盤として，数十万種の一塩基多型（single nucleotide polymorphism：SNP）を数千もの個体について並列解析できるプラットフォームが市販化された。

HapMap計画によると，日本人と白人は約25万～30万個のタグSNP（これを調べれば連鎖不平衡で結ばれた近傍の多くのSNPの代表になる）で，ほぼ全ゲノムの遺伝子がカバーされる。つまり約30万個のタグSNPを患者と対照で調べれば，ほぼ全ゲノムの遺伝子を調べたことになる。そこで具体的には，例えば患者1,000人，対照1,000人，計2,000人のそれぞれ50万個のSNPの遺伝子型を決定する。すなわちSNPチップとして2,000枚の実験を行う。それぞれSNP-1，SNP-2，……，SNP-500000ずつ，患者，対照におけるそれぞれのアレルの出現頻度を合計し，偏りがないかどうかの検定を行うのである。

これらを活用することによって，GWASが実用的な戦略となり，2007年には『Nature』『Science』誌などに立て続けに成果が発表されることとなった。その後のGWASによる疾患感受性遺伝子の発見ラッシュには目を見張るものがあり，すでに200以上の疾患について，ゲノムワイド有意水準$P<5\times10^{-8}$をクリアする1,000編以上の論文が発表されている。

パーキンソン病を例にとると，筆者らのグループは患

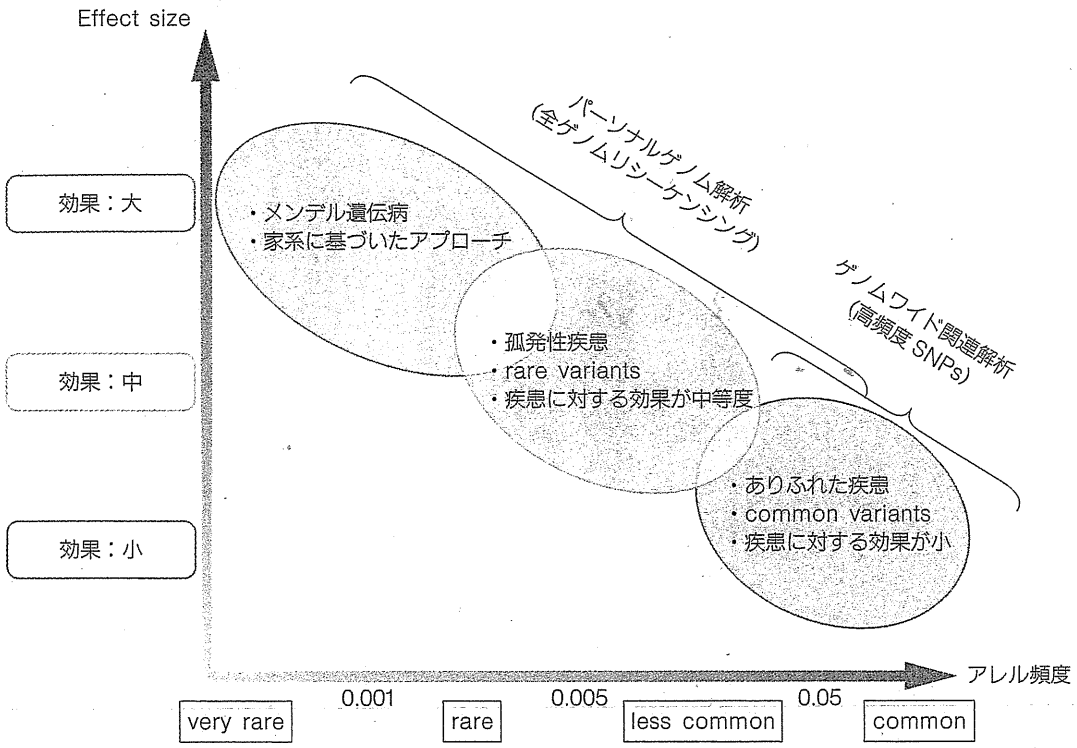

Fig. 1　一般集団における variant の頻度と効果の関係およびそのアプローチのしかた
左上が単一遺伝性疾患における変異，右下が SNP，中間が rare variant を表す。
Tsuji S: Genetics of neurodegenerative diseases: insights from high-throughput resequencing. Hum Mol Genet **19**(R1): R65-70, 2010 から改変して転載

者の 95%を占める孤発性パーキンソン病のリスク遺伝子を同定するため GWAS を行い，パーキンソン病発症に関わる 2 つの新しい遺伝子座 *PARK16*，*BST1* を同定した。また，常染色体優性遺伝性パーキンソン病の原因遺伝子 *α-synuclein*，*LRRK2* の孤発性パーキンソン病への関与を証明した[5]。

さらにパーキンソン病においては，さらなる国際共同研究として欧米の 5 つのグループがそれぞれ独立に行っていた GWAS を合わせてメタ解析を行い（計患者 5,333，対照 12,019），有意な SNP をさらに患者 7,053，対照 9,007 で再現実験を行い，ゲノムワイド有意水準 $P<5\times10^{-8}$ を超える遺伝子を従来の 6 個のほかに，*ACMSD*，*STK39*，*LAMP3*，*SYT11*，*CCDC62* の 5 個同定した[6]。このような圧倒的な数の試料を各地から集めてゲノムワイドメタ解析を行い，より効果サイズの小さなものも同定するという試みが行われだしており，「第 2 世代の GWAS」ともいわれている。

しかしながら，このような，頻度の高い common SNPs を用いて見出される疾患感受性遺伝子のオッズ比は多くの場合 2 以下と，あまり大きくなく，疾患の病態機序の全貌を明らかにするには至っていない（missing heritability）[4,7]。

Ⅳ. Missing heritability（失われた遺伝性）と common disease-multiple rare variants 仮説

GWAS によって多数の疾患感受性遺伝子が同定されたものの，それらは遺伝要因全体の一部しか説明できない。

一方，単一遺伝子疾患と多因子疾患の間には，単一遺伝子疾患における病因変異ほどではないものの，オッズ比の高い変異が関与する疾患が存在する可能性が考えられる。このような考え方は，common disease-multiple rare variants 仮説と呼ばれる。

ゴーシェ病は，常染色体劣性遺伝性疾患で，リソソーム内酵素 GBA（グルコセレブロシダーゼ）の遺伝子 *GBA* の変異による酵素活性低下により，グルコシルセラミドをセラミドに分解できず，グルコシルセラミドが体内に蓄積し，肝脾腫，貧血，出血傾向，骨疾患などを引き起こす脂質代謝異常症である。一見，パーキンソン病とはなんの関係もない疾患ではあるが，1990 年代後

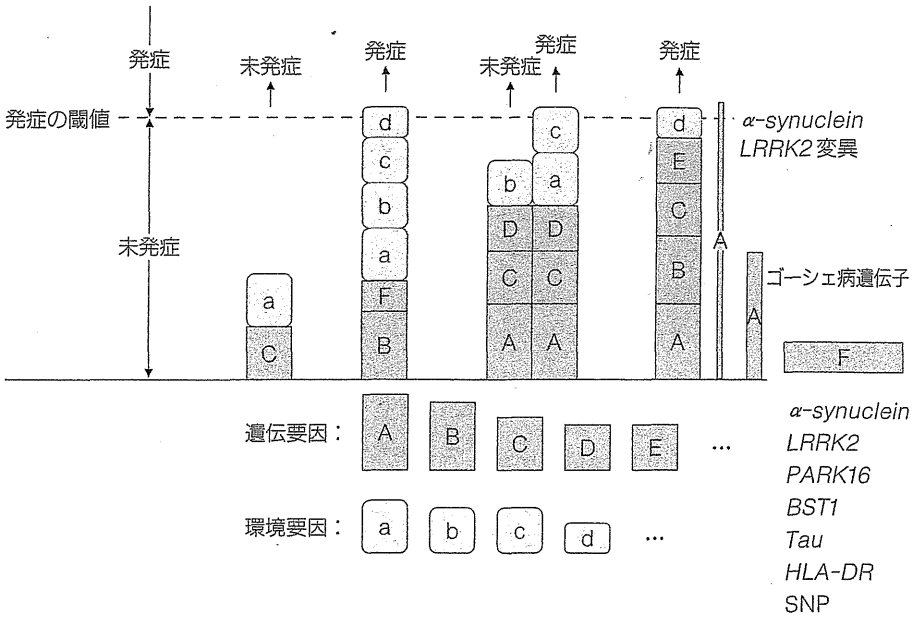

Fig. 2　孤発性神経疾患のモデル

パーキンソン病，アルツハイマー病，または生活習慣病を含むほとんどの疾患は，複数の遺伝因子と複数の環境因子の積み木の総和が，ある閾値を超えたとき発症すると考えられている。メンデル遺伝性変異以外に，common variant として *α-synuclein*，*PARK16*，*BST1*，*LRRK2*，*Tau*，*HLA-DR* の SNP が，また rare variant としてゴーシェ病遺伝子が重要である。

半からパーキンソン病症状を合併するゴーシェ病患者の存在や，ゴーシェ病家系内にパーキンソン病患者が多発するとの報告が散見されていた。そこで，Aharon-Peretz らは，ユダヤ人のパーキンソン病患者について *GBA* 変異の頻度を調べたところ，孤発性パーキンソン病群では，*GBA* 変異のヘテロ保因者が対照群に比べ有意に多く，*GBA* が孤発性パーキンソン病のリスク遺伝子であることを報告した。

その後，この研究の再現研究が世界中で行われ，東京大学と筆者らの共同研究グループも，*GBA* 変異が，日本人でもパーキンソン病感受性を持つことを示す[8]と同時に，世界多施設共同研究に参画，アメリカ人，フランス人，ポルトガル人，台湾人などを含む計約 10,000 人の患者対照集団とのメタ解析により，原著のユダヤ人に限らず，どの人種でも *GBA* 遺伝子はリスクとなり，平均オッズ比は 5 であり，確実なパーキンソン病リスク遺伝子であることが示された[9]。GBA の基質であるグルコシルセラミドの蓄積により，神経毒性を持つとされる可溶性 α シヌクレインオリゴマーが増加すること，可溶性 α シヌクレインオリゴマーの増加により GBA の小胞体-ゴルジ輸送が阻害されることによりさらに GBA 活性が低下し，可溶性 α シヌクレインオリゴマーのさらなる増加につながる，といったポジティブフィードバックの経路が最近報告され，興味深い[10]。

パーキンソン病症例では，多様な *GBA* のヘテロ接合性変異が見出されており，このような変異は，common SNPs を用いた GWAS では見出しえないもので，リシーケンシングを行ってはじめて見出されたという点に注目したい。

パーキンソン病，アルツハイマー病，または生活習慣病を含むほとんどの疾患は，複数の遺伝因子と複数の環境因子の積み木の総和がある閾値を超えたとき発症すると考えられている。そのモデルをパーキンソン病を例にとり Fig. 2 に示す。メンデル遺伝性パーキンソン病を引き起こす *α-synuclein* や *LRRK2* の変異はそれ 1 つだけで閾値に到達し発症するが，対象患者はほとんど存在しないので積み木の幅はとても狭い（とても稀）。ゴーシェ病遺伝子 *GBA* などの rare variant リスクは中等度の高さを持つが，10%以下の患者にしか当てはまらないため幅は狭い。一方，SNP はそれ自体のオッズ比は低いがほとんどの患者に当てはまるため，積み木の幅は広い。いずれも重要である。

V．次世代シーケンサーの実用化

現在，次世代シーケンサーという言葉はあちこちで聞

Table　各種次世代シーケンサーのスループット

機種	リード数	リード長	解析塩基数	稼働時間
イルミナ社				
GAIIx	～3億2,000万	150＋150	96 Gb	～14日
HiSeq2500	～60億	100＋100	600 Gb	～11日
MiSeq	～3,400万	250＋250	6～7 Gb	～39時間
ロシュ社				
GS FLX Titanium XL＋	100万	700	700 Mb	23時間
GS FLX Titanium XLR70	100万	450	450 Mb	10時間
GS junior	10万	～400	～35 Mb	12時間
ライフテクノロジーズ社				
5500xl SOLiD	＞14億	75＋35	～180 Gb	8日
Ion PGM	～500万	＞100	～1 Gb	～6.8時間
Ion Proton	～8,000万	200	～10 Gb	2～4時間
パシフィックバイオサイエンス社				
PacBio RS	1万	＞3,000	5～10 Mb	3.5時間

くし，この特集のテーマにもなっている。次世代シーケンサーには主としてイルミナ社，ロシュ社，ライフテクノロジーズ社のものがあり，それぞれ異なる原理での解析を行っており，また1分子シーケンスと超ロングリードを売りにして2011年に発売されたパシフィックバイオサイエンス社もある。それぞれTableに示すようなスループットを持っている。2003年には1人のゲノムを読むのに，30億ドルの費用と13年の年月がかかったが，今や1回の稼動でヒトゲノム3 Gb（1人分）の200倍に相当するような量が読めるのである。

さらに全エクソンをビーズで濃縮してエクソンとその周辺を読むエクソーム解析（Fig. 3）と，全ゲノム配列を読む全ゲノム解析がある。ヒトの全ゲノムのリシーケンシングはコスト的にはまだまだ高額であり，現時点ではエクソーム解析が主流であるが，濃縮できない配列もあり，ゲノム解析の技術の進歩には目を見張るものがあるので，将来は全ゲノム解析が中心になると思われる。いわゆる“1,000ドルゲノム”の時代の到来も近い。

代表的なイルミナ社の解析原理を示すと（Fig. 4），Genome Analyzer（GA）IIxやHiSeq，MiSeqでは，ブリッジPCRという方法を用いて，一本鎖DNA断片のクラスターをフローセル表面に作る。解析の際は，まずサンプルから得たDNA断片の両端に，2種類のアダプター配列（アダプター1，2）を連結させる。それを一本鎖にして，5′末端（アダプター1の側とする）をフローセル上に固定する。フローセル上には，あらかじめアダプター1，2と相補的に結合するプライマーが高密度に配置されており，サンプルの一本鎖DNAはアダプター2の側でこのプライマーと補助的に統合することになる（橋がかかったような構造になる）。この状態でDNAポリメラーゼによる伸長反応のあとに変性させると，フローセル上にはアダプター1側で結合した一本鎖と，アダプター2側で結合した一本鎖ができあがる。この反応を繰り返すことで，狭い面積の中で一本鎖DNAを固定しながら増幅することができる（Fig. 4）。これを鋳型として配列解析を行う。

塩基配列の解析には，蛍光標識したdNTPの取り込みを蛍光顕微鏡によって解析する。このdNTPは3′末端がブロックされており，1回の伸長反応で1塩基しか延ばせない。そのため，1塩基ごとにどのdNTPが取り込まれたかを観察し，蛍光物質とブロックを外して次の伸長反応を行うというステップで，解析を進めていく。シングルリード法ではアダプター1の側からのみ，ペアエンド法ではアダプター1の側と2の側からそれぞれ最大で150 bpを解析可能となっている（Fig. 5）。

ヒトなどサイズの大きなゲノムを解析する場合，当然シーケンサーにも大きな総解析塩基数を求められる。イルミナ社のGAIIxやHiSeqが現在市場をリードしているのも，圧倒的な総解析塩基数と，ポリメラーゼによる伸長反応というスタンダードな解析原理を採用しているが故にヒトゲノムのリシーケンスなどに強いためであろう。最近では，イルミナ社のMiSeqやライフテクノロジーズ社のIonシリーズ，ロシュ社のGS juniorなど，総解析塩基数を抑え，アプリケーションを絞る代わりにコストが低く稼働時間が短い次世代シーケンサーが増えている。

VI. 次世代シーケンサーの神経疾患研究への応用

さて，ではこのように隆盛の次世代シーケンサーをど

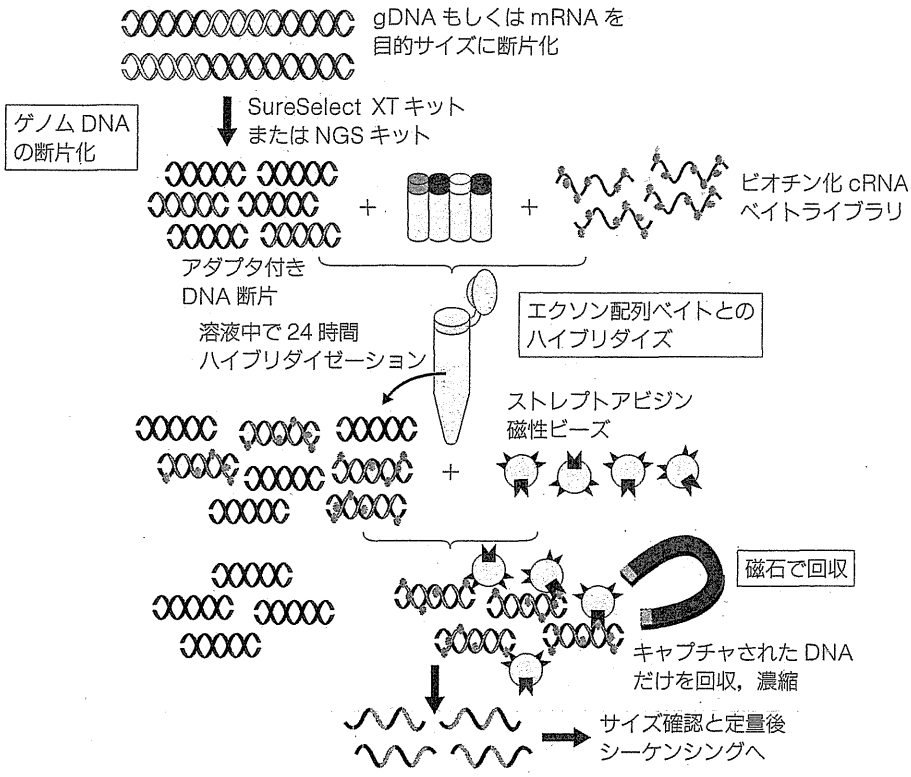

Fig. 3　エクソーム解析の原理

ビーズに全遺伝子の全エクソン配列にほぼ対応するヌクレオチドが搭載されており，解析サンプル DNA を断片化しビーズにハイブリダイズすると，エクソン部分だけが濃縮できる。

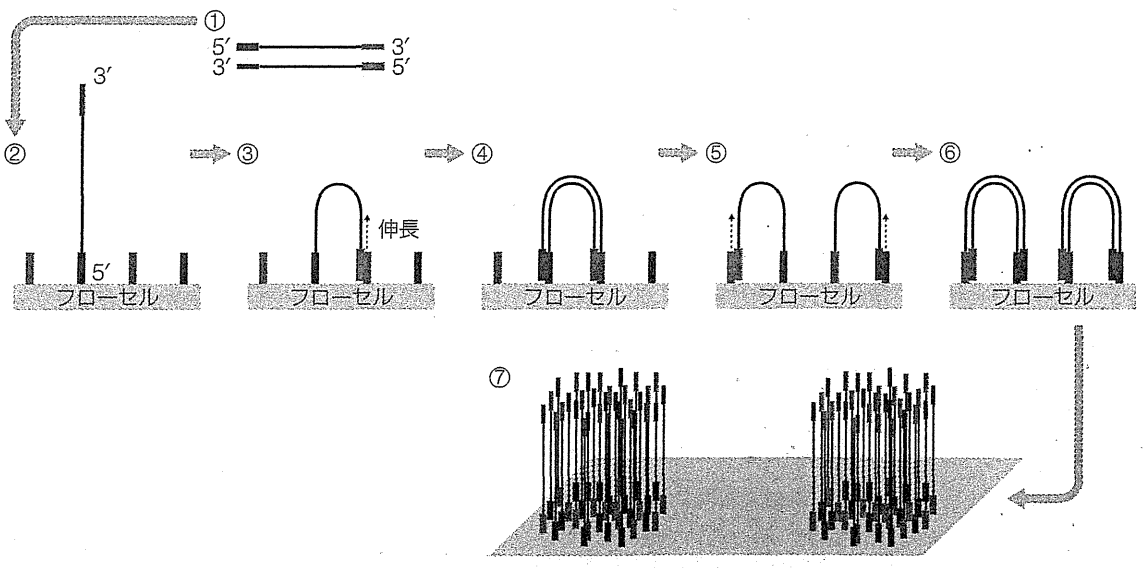

Fig. 4　イルミナ方式（ブリッジ PCR）の原理

サンプル由来の DNA 断片（黒線）の両端にアダプター配列を付加し，5′ 側アダプター配列を固定したフローセルの上で伸張反応を繰り返す。すると同じ DNA 断片由来のコピー配列が近くに密集し，クラスターを形成する。